

University of Mississippi

eGrove

---

Electronic Theses and Dissertations

Graduate School

---

1-1-2020

## Determining The Effectiveness Of Rock Mass Classification Schemes When Used To Derive Empirical Predictions For Rock Mass Deformation Modulus

Tanner Cecil Avery

Follow this and additional works at: <https://egrove.olemiss.edu/etd>

---

### Recommended Citation

Avery, Tanner Cecil, "Determining The Effectiveness Of Rock Mass Classification Schemes When Used To Derive Empirical Predictions For Rock Mass Deformation Modulus" (2020). *Electronic Theses and Dissertations*. 1855.

<https://egrove.olemiss.edu/etd/1855>

This Thesis is brought to you for free and open access by the Graduate School at eGrove. It has been accepted for inclusion in Electronic Theses and Dissertations by an authorized administrator of eGrove. For more information, please contact [egrove@olemiss.edu](mailto:egrove@olemiss.edu).

DETERMINING THE EFFECTIVENESS OF ROCK MASS CLASSIFICATION SCHEMES  
WHEN USED TO DERIVE EMPIRICAL PREDICTIONS FOR ROCK MASS  
DEFORMATION MODULUS

A Thesis

Presented in partial fulfillment of requirements

Masters of Science

Degree

The University of Mississippi

Tanner Avery

May 2020

Copyright © 2020 by Tanner Avery  
All rights reserved

## ABSTRACT

Normal deformation modulus of rock masses ( $E_{rm}$ ) is a critical design parameter for any permanent excavation and infrastructure project that requires limited or controlled deformations to ensure performance of permanent support systems and of foundations. Despite being a key parameter, the optimal methods for determining  $E_{rm}$  is still debated. These methods can be put into three categories: in-situ tests, empirical solutions, and numerical solutions. Current efforts to derive empirical predictions rely on rock mass classification schemes (RMCS) with the assumption that all RMCS are similarly effective at predicting  $E_{rm}$ . Since different RMCS use different sets of variables this assumption does not likely hold true as a single RMCS value can be representative of a wide range of rock mass conditions. This study is an attempt to explore the effectiveness of various classification systems and their constituting parameters.

## DEDICATION

I would like to dedicate this thesis to all the members of my family who helped mold me into the man I am today. Without the love and support they have given me I would have never been able to achieve what I have. For teaching me the importance of hard work, love, compassion, and seeing things through until the end, thank you.

## LIST OF SYMBOLS AND ABBREVIATIONS

a	Constant from the Hoek Brown Failure Criterion
b	Constant from the Hoek Brown Failure Criterion
D	Disturbance Factor
DEM	Discrete Element Method
$d_i$	Initial borehole diameter
$E_i$	Deformation modulus of intact rock.
$E_{rm}$	Rock mass deformation modulus
f	Instrument correction factor
FEM	Finite Element Method
GSI	Geological Strength Index
$J_a$	Joint alteration factor
jC	Joint condition factor
JCS	Joint Compressive Strength
jL	Joint length
$J_n$	Joint number
$J_P$	Jointing parameter of intact rock
$j_R$	Joint roughness factor (R <sub>Mi</sub> )
$J_r$	Joint roughness number
JRC	Joint Roughness Coefficient

$j_s$	Small scale joint roughness
$J_v$	Joint volume count
$J_w$	Joint weathering factor
$j_w$	Large scale joint roughness (Waviness)
$m_i$	Material Constant from Hoek Brown failure Criterion
$Q$	Q System
$Q_c$	Normalized Q rating
RMCS	Rock Mass Classification Scheme(s)
RMi	Rock Mass Index
RMR	Rock Mass Rating
RQD	Rock Quality Designation
RS2	RocScience finite element modeling software
SRF	Strength reduction factor
UCS	Uniaxial compressive strength
$V_b$	Block Volume
$\Delta d$	Change in borehole diameter
$\Delta h$	Separation of load plates
$\Delta P_i$	Change in contact pressure over load plate area
$\Delta p_d$	Effective dilation pressure

$\sigma_c$  Uniaxial compressive strength

$\Phi$  Angle of Internal Friction

## ACKNOWLEDGMENTS

I would like to thank Dr. Adnan Aydin at the University of Mississippi. Without his knowledge and guidance this thesis would not be possible.

## TABLE OF CONTENTS

CHAPTER I.....	1
INTRODUCTION.....	1
CHAPTER II.....	4
<b>I. Rock Mass Rating Systems</b> .....	4
Rock Quality Designation (RQD) System.....	4
RMR System .....	4
Q System .....	5
Geological Strength Index (GSI) .....	10
Rock Mass Index (RMi).....	10
<b>II. Approaches to Finding <math>E_{rm}</math></b> .....	13
Numerical modeling has become more popular in recent years due to significant increases in computing power (JianPing et al, 2015). Numerical methods can be divided into two categories; finite element method (FEM) and discrete element method (DEM). While FEM modeling has been used, they have difficulty modeling the discontinuities present in a rock mass. Joint elements have been included in FEM in order to more accurately model the effect of discontinuities.....	14
Field Test .....	14
Plate Jacking Test .....	14
Borehole Test.....	16

Flat Jack Test .....	19
Pressure Tunnel and Radial Jacking Test .....	19
Tunnel Relaxation Test.....	20
Dynamic Test.....	20
Stress Relief Test .....	21
Numerical Modeling.....	21
Finite Element Method (FEM) .....	21
Discrete Element Method (DEM).....	22
CHAPTER III .....	24
<b>I. Selection of Formulas</b> .....	24
<i>Galera et al, 2005</i> .....	24
Barton, 2002 .....	25
Barton et al, 1983.....	26
Beiki et al, 2010.....	27
Hoek and Diederichs, 2006 .....	29
Palmström and Singh, 2001 .....	30
Read et al, 1999 .....	31
<b>II. Building and Validating the Numerical Models</b> .....	32

Common characteristics between models .....	35
RMR30 Models.....	36
RMR45 Models.....	37
RMR60 Models.....	37
RMR75 Models.....	38
Model Validation.....	38
<b>III. Testing the Formulas.....</b>	<b>40</b>
<b>CHAPTER IV .....</b>	<b>43</b>
<b>I. Analytical vs Numerical Stress Patterns .....</b>	<b>43</b>
<b>II. <math>E_{rm}</math> Predictions .....</b>	<b>43</b>
<b>CHAPTER V .....</b>	<b>53</b>
<b>I. Geologic Setting.....</b>	<b>53</b>
<b>II. Building the In Situ Model .....</b>	<b>54</b>
In situ measurements .....	54
Stage 1 model Parameters.....	54
Stage 2 Model Parameters.....	56
Stage 3 Model Parameters.....	58

<b>III. Results and Discussion</b> .....	60
CHAPTER VI .....	62
DISCUSSION AND CONCLUSION .....	62
Appendix A .....	65
Appendix B .....	66
VITA .....	74

## LIST OF TABLES

Table 1-1. Selected empirical predictive relationships for $E_{rm}$ .....	3
Table 3-1. Galera et al (2005) data Set.....	25
Table 3-2. Barton (2002) data set.....	26
Table 3-3. Barton (1983) data set.....	27
Table 3-4. Beiki et al (2010) data set.....	28
Table 3-5. Hoek and Diederichs (2006) data set.....	30
Table 3-6. Read et al (1999) data set.....	31
Table 3-7. Variables accounted for in each RMCS.....	34
Table 3-8. RMR ratings for each model.....	34
Table 3-9. Joint properties of each model.....	36
Table 3-10. Properties of intact rock not given by RMR.....	42
Table 3-11. Predictive relations between RMCS.....	42
Table 3-12. RMCS value for each model.....	40
Table 3-13. Predictive formula results.....	41
Table 4-1. Predictive formula results.....	44
Table 5-1. Peak and residual strength parameters for fractured rock.....	55
Table 5-2. Ultrasonic pulse test results.....	55
Table 5-3. Parameters for discontinuities.....	57
Table 5-4. Peak and residual strength parameters for massive rock.....	57

Table 5-5 Predicted Erm for case study.....59

Table 6-1. Angles at which maximum and minimum deformations occurred in each model  
set.....62

## LIST OF FIGURES

<b>Figure 2-1.</b> RMR table (Bieniawski, 1989).....	6
<b>Figure 2-2.</b> Table for determining $J_n$ values (Barton, 2006).....	5
<b>Figure 2-3.</b> Examples for $J_n$ values given as block diagrams and stereo nets (NGI, 2015).....	7
<b>Figure 2-4.</b> Chart for determining $J_r$ value (Barton, 2006).....	7
<b>Figure 2-5.</b> Table for determining $J_a$ values (Barton, 2002).....	8
<b>Figure 2-6.</b> Table for determining $J_w$ values (Barton, 2002).....	8
<b>Figure 2-7.</b> Table for finding SRF rating (Barton, 2002).....	9
<b>Figure 2-8.</b> Basic structure of GSI chart (Hoek and Marinos, 2000).....	10
<b>Figure 2-9.</b> Descriptions for determining $j_s$ (Palmström, 1996).....	11
<b>Figure 2-10.</b> Descriptions for visually determining $j_w$ (Palmström, 1996).....	11
<b>Figure 2-11.</b> Tables for determining the joint alteration factor for RMI system.....	12
<b>Figure 2-12.</b> Tables for determining the joint length parameter for RMI (Palmström, 1996).....	12
<b>Figure 2-13.</b> Plate jacking test (Rezaei et al, 2016).....	14
<b>Figure 2-14.</b> Diagram of plate jacking test and damage zones. (Hoek and Diederichs, 2006)....	15
<b>Figure 2-15.</b> Application range of various types of borehole deformation probes (Sharma and Saxena, 2002).....	16
<b>Figure 2-16.</b> Dilatometer Test (Marchetti et al, 2001).....	17

<b>Figure 2-17.</b> Sketch of a Ménard pressuremeter (Baguelin et al., 1972).....	17
<b>Figure 2-18.</b> Flat jack to be inserted into rock mass (Hoek and Diederichs, 2006).....	18
<b>Figure 2-19.</b> Types of elements for FEM (Moreno, 2011).....	21
<b>Figure 2-20.</b> Representation of rock mass using DEM. Blue particles represent intact rock while green particles represent a joint (Ivars et al, 2011).....	23
<b>Figure 3-1.</b> Plot of Hoek and Brown (2006) equation with in-situ data from China and Taiwan (Hoek and Diederichs, 2006).....	29
<b>Figure 3-2.</b> Model with boundary conditions.....	35
<b>Figure 3-3.</b> Diagram of X, Y, $\alpha$ , $\beta$ , and $\theta$ for equation 2 (Goodman, 1989).....	39
<b>Figure 3-4.</b> Mapped points used for contours in analytical solution.....	39
<b>Figure 3-5.</b> Empirical relations between Q and RMR rating along with Q and RMR values from Table 6.....	40
<b>Figure 3-6.</b> Total deformations will be mapped out along the center line of the model (red line) and along the surface (black line).....	40
<b>Figure 4-1.</b> Comparison of analytical (left) and numerical (right) vertical stress distribution for models with discontinuities tilted 0°, 30°, 45°, 60°, and 90° from the surface.....	43
<b>Figure 4-2.</b> Maximum and minimum total deformations along the center line of the distributed load of each numerical model of RMR30 rock mass along with predicted deformations by the selected empirical formulas Table (1-1).....	45

**Figure 4-3.** Maximum and minimum total deformations along the surface of each numerical model of RMR30 rock mass along with the predicted deformations by the selected empirical formulas Table (1-1).....46

**Figure 4-4.** Maximum and minimum total deformations along the center line of the distributed load of each numerical model of RMR45 rock mass along with predicted deformations by the selected empirical formulas Table (1-1).....47

**Figure 4-5.** Maximum and minimum total deformations along the surface of each numerical model of RMR45 rock mass along with the predicted deformations by the selected empirical formulas Table (1-1).....48

**Figure 4-6.** Maximum and minimum total deformations along the center line of the distributed load of each numerical model of RMR60 rock mass along with predicted deformations by the selected empirical formulas Table (1-1).....49

**Figure 4-7.** Maximum and minimum total deformations along the surface of each numerical model of RMR60 rock mass along with the predicted deformations by the selected empirical formulas Table (1-1).....50

**Figure 4-8.** Maximum and minimum total deformations along the center line of the distributed load of each numerical model of RMR30 rock mass along with predicted deformations by the selected empirical formulas Table (1-1).....51

<b>Figure 4-9.</b> Maximum and minimum total deformations along the surface of each numerical model of RMR75 rock mass along with the predicted deformations by the selected empirical formulas Table (1-1).....	52
<b>Figure 5-1.</b> Roadcut modeled in RS2.....	53
<b>Figure 5-2.</b> Road cut with measured surfaces for discontinuity survey labeled.....	54
<b>Figure 5-3.</b> Stage 1 model with boundary conditions.....	54
<b>Figure 5-4.</b> Stage 2 model. Fractured rock is shown in purple, massive rock in green, and the fault is shown by the orange line (Mesh size is reduced in order to display model features).....	56
<b>Figure 5-5.</b> Kaolin infill of the fault.....	56
<b>Figure 5-6.</b> Total deformations for each predictive formula and the modeled outcrop.....	60

## CHAPTER I INTRODUCTION

Normal deformation modulus of rock masses ( $E_{rm}$ ) is a critical design parameter for any excavation or construction project that needs to account for deformations in rock.  $E_{rm}$  is an important parameter when designing rock mass simulations to predict stress distributions and deformation behaviors. Despite its importance, the best way to efficiently determine this parameter is still debated among researchers. There are a variety of competing approaches to find  $E_{rm}$  (empirical, analytical, numerical, and in situ) (Zhang, 2017).

This thesis focuses on the effectiveness of the empirical approach for predicting  $E_{rm}$  in transversely isotropic rock masses. While empirical predictive formulas use different mathematical structures and variables, they are all based on a rock mass classification scheme (RMCS) most common of which are RMR, RMI, Q, and GSI. Use of a RMCS offer the ability to represent the rock mass condition with a single variable. There are currently more than 30 different proposed empirical methods for determining  $E_{rm}$  (Shen et al, 2012; Kayabasi and Gokceoglu, 2018; Zhang, 2017). With so many different formulas current research is becoming repetitive and progress stagnant. By investigating the effectiveness of these four RMCS this study seeks to determine which RMCS is more efficient in deriving successful predictive formulas for  $E_{rm}$ . The ultimate result of this research is to give future research a way to move forward.

Among many, eight different empirical formulas are selected for this investigation (Table 1-1). Each of the four RMCS is used as a base in two these formulas. Twenty-four numerical

models are built using a finite element software in order to test how successful each predictive formula performs. These models are transversely isotropic synthetic rock masses designed to simulate realistic rock mass conditions at varying RMCS values. These models are checked by visually comparing the stress distribution patterns produced by these numerical models with the results of an analytical solution (Goodman, 1989) that predicts stress distributions in transversely isotropic rock masses. A high degree of consistency between the patterns produced by two independent methods confirm the validity of numerical models.

Once each model is verified the displacements in the model are compared to the displacements based on the predicted  $E_{rm}$  given by the formulas in table 1-1. An additional finite element model (FEM) of a roadcut in Hardy Arkansas is set up as a case study to see how the predictions perform in rock masses with a more complex structure than transversely isotropic. This scope of this paper will cover the current methods used for classifying rock masses, methods for estimating  $E_{rm}$ , methodologies for choosing which empirical formulas to test and how to test them, and the results from numerical simulations performed to see the predictive capabilities of four different rock mass classification systems when used to derive equations for predicting  $E_{rm}$ . The background section of this thesis contains information on the origin and use of each rock mass classification scheme along with alternative used to estimate  $E_{rm}$ . The methods for predicting  $E_{rm}$  covered are in situ test, empirical predictions, and numerical modeling. Additionally, the way each formula was chosen and details of each formula are discussed. In the methods section, construction and verification of the numerical models is discussed along with the processes used for evaluating the effectiveness of the formulas. Results from the test performed in this thesis can be found in the discussion and conclusion section.

Table 1-1. Selected empirical predictive relationships for  $E_{rm}$

Author	Formula	Limitations
Barton, 1983	$E_{rm} = 25 \log(Q)$	$Q > 1$
Barton, 2002	$E_{rm} = 10 \left( Q \frac{\sigma_c}{100} \right)^{\frac{1}{3}}$	
Beiki et al, 2010	$E_{rm} = \tan(1.56 + \ln GSI^2)^{\frac{1}{2}} * (\sigma_c)^{\frac{1}{3}}$	
Galera et al, 2005	$E_{rm} = E_i e^{\frac{(RMR-100)}{36}}$	
Hoek and Diedrichs, 2006	$E_{rm} = 100,000 \left( \frac{1 - \left(\frac{D}{2}\right)}{1 + e^{\frac{(75+15D-GSI)}{11}}} \right)$	
Palmstrom and Singh, 2001	$E_{rm} = 5.6 RMi^{0.375}$ $E_{rm} = 7 RMi^{0.4}$	$0.1 < RMi < 1$ $1 < RMi < 30$
Read et al, 1999	$E_{rm} = 0.1 \left( \frac{RMR}{10} \right)^3$	

$\sigma_c$  = Uniaxial compressive strength

D = Disturbance factor

$E_i$  = Intact Elastic Modulus

## CHAPTER II BACKGROUND

### I. Rock Mass Rating Systems

#### *Rock Quality Designation (RQD) System*

Deere et al (1967) proposed the RQD system. RQD is found by taking a rock core and determining the percentage of intact core pieces longer than 10 cm within the total length of the core. The core should be at least 54.7 mm in diameter and should be drilled with a double core barrel. If no borehole is available Palmström et al, (1982) provides an equation to determine RQD using discontinuity traces on the joint surface represented by joint volume count ( $J_v$ ) (EQ. 2-1).

$$RQD = 115 - 3.3 * J_v \quad (2-1)$$

While RQD is not used much today to describe a rock mass it is an important parameter in more modern rating systems.

#### *RMR System*

This rating system was first proposed by Bieniawski (1973) to aid in the design of tunnels in hard and soft rock. It is based on a review of 49 case records (Bieniawski, 1989). A revision was made in 1989 after more data was available (Cai, 2006). Today, RMR is used in a wide range of engineering projects such as: slopes, tunnels, mines, and foundations. There are six

parameters used to classify rock mass: Uniaxial compressive strength of rock material ( $\sigma_c$ ), rock quality designation, joint spacing, joint condition, groundwater conditions, and joint orientation (Fig 2-1.). The final rating is found by the sum of each factor's individual rating which is determined by using an RMR table (Fig. 2-1) (Bieniawski, 1989). The ratings for the RMR system give a range of values from 100 to 20 with anything with a rating less than 20 being considered very poor rock (Barton, 2002).

When using the RMR classification scheme the rock mass is divided into separate structural differences. The boundaries of these regions should coincide major structural features such as faults, dikes, and shear zone (Bieniawski, 1989).

### *Q System*

After evaluating 212 case histories from Scandinavia, Barton et al (1974) proposed a Tunnel Quality Index (Q) for determining rock mass characteristics and tunnel support requirements.

Massive, no or few joints	$J_n = 0.5 - 1$
One joint set	2
One joint set plus random	3
Two joint sets	4
Two joint sets plus random joints	6
Three joint sets	9
Three joint sets plus random joints	12
Four or more joint sets, heavily jointed, "sugar-cube", etc.	15
Crushed rock, earthlike	20

**Figure 2-2.** Table for determining  $J_n$  values (Barton, 2006).

The Q system was later updated in Grimstad and Barton (1998) and once more with Barton (2002) adding minor changes to SRF ratings. The Q system is based on six different parameters: rock quality designation (RQD), joint set number ( $J_n$ ), joint roughness number ( $J_r$ ), joint alteration number ( $J_a$ ), joint water reduction factor ( $J_w$ ), and stress reduction factor. The method for determining Q is given by equation 2-2. Q values range from 0.001 to 1000 and

$$Q = \frac{RQD}{J_n} * \frac{J_r}{J_a} * \frac{J_w}{SRF} \quad (2-2)$$

encompass rock mass qualities from heavy squeezing ground to solid unjointed rock (Barton et

A. CLASSIFICATION PARAMETERS AND THEIR RATINGS									
Parameter			Range of values						
1	Strength of intact rock material	Point-load strength index	>10 MPa	4 - 10 MPa	2 - 4 MPa	1 - 2 MPa	For this low range - uniaxial compressive test is preferred		
		Uniaxial comp. strength	>250 MPa	100 - 250 MPa	50 - 100 MPa	25 - 50 MPa	5 - 25 MPa	1 - 5 MPa	< 1 MPa
		Rating	15	12	7	4	2	1	0
2	Drill core Quality RQD		90% - 100%	75% - 90%	50% - 75%	25% - 50%	< 25%		
	Rating		20	17	13	8	3		
3	Spacing of		> 2 m	0.6 - 2 . m	200 - 600 mm	60 - 200 mm	< 60 mm		
	Rating		20	15	10	8	5		
4	Condition of discontinuities (See E)		Very rough surfaces Not continuous No separation Unweathered wall rock	Slightly rough surfaces Separation < 1 mm Slightly weathered walls	Slightly rough surfaces Separation < 1 mm Highly weathered walls	Sticksided surfaces or Gouge < 5 mm thick or Separation 1-5 mm Continuous	Soft gouge >5 mm thick or Separation > 5 mm Continuous		
	Rating		30	25	20	10	0		
5	Groundwater	Inflow per 10 m tunnel length (l/m)	None	< 10	10 - 25	25 - 125	> 125		
		(Joint water press)/ (Major principal $\sigma$ )	0	< 0.1	0.1, - 0.2	0.2 - 0.5	> 0.5		
	General conditions		Completely dry	Damp	Wet	Dripping	Flowing		
	Rating		15	10	7	4	0		
B. RATING ADJUSTMENT FOR DISCONTINUITY ORIENTATIONS (See F)									
Strike and dip orientations			Very favourable	Favourable	Fair	Unfavourable	Very Unfavourable		
Ratings	Tunnels & mines		0	-2	-5	-10	-12		
	Foundations		0	-2	-7	-15	-25		
	Slopes		0	-5	-25	-50			
C. ROCK MASS CLASSES DETERMINED FROM TOTAL RATINGS									
Rating	100 ← 81		80 ← 61	60 ← 41	40 ← 21	< 21			
Class number	I		II	III	IV	V			
Description	Very good rock		Good rock	Fair rock	Poor rock	Very poor rock			
D. MEANING OF ROCK CLASSES									
Class number	I		II	III	IV	V			
Average stand-up time	20 yrs for 15 m span		1 year for 10 m span	1 week for 5 m span	10 hrs for 2.5 m span	30 min for 1 m span			
Cohesion of rock mass (kPa)	> 400		300 - 400	200 - 300	100 - 200	< 100			
Friction angle of rock mass (deg)	> 45		35 - 45	25 - 35	15 - 25	< 15			
E. GUIDELINES FOR CLASSIFICATION OF DISCONTINUITY conditions									
Discontinuity length (persistence)	< 1 m		1 - 3 m	3 - 10 m	10 - 20 m	> 20 m			
Rating	6		4	2	1	0			
Separation (aperture)	None		< 0.1 mm	0.1 - 1.0 mm	1 - 5 mm	> 5 mm			
Rating	6		5	4	1	0			
Roughness	Very rough		Rough	Slightly rough	Smooth	Sticksided			
Rating	6		5	3	1	0			
Infilling (gouge)	None		Hard filling < 5 mm	Hard filling > 5 mm	Soft filling < 5 mm	Soft filling > 5 mm			
Rating	6		4	2	2	0			
Weathering	Unweathered		Slightly weathered	Moderately weathered	Highly weathered	Decomposed			
Ratings	6		5	3	1	0			
F. EFFECT OF DISCONTINUITY STRIKE AND DIP ORIENTATION IN TUNNELLING**									
Strike perpendicular to tunnel axis					Strike parallel to tunnel axis				
Drive with dip - Dip 45 - 90°			Drive with dip - Dip 20 - 45°		Dip 45 - 90°		Dip 20 - 45°		
Very favourable			Favourable		Very unfavourable		Fair		
Drive against dip - Dip 45-90°			Drive against dip - Dip 20-45°		Dip 0-20 - Irrespective of strike*				
Fair			Unfavourable		Fair				

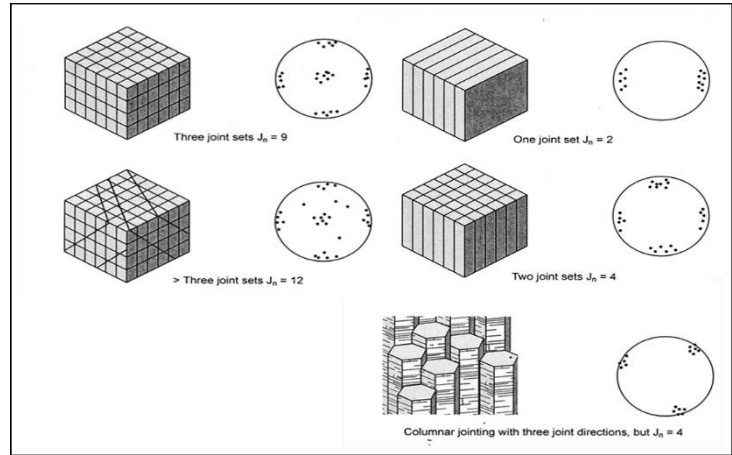
Some conditions are mutually exclusive . For example, if infilling is present, the roughness of the surface will be overshadowed by the influence of the gouge. In such cases use A.4 directly.  
\*\* Modified after Wickham et al (1972).

Figure 2-1. RMR table (Bieniawski, 1989)

al, 1973).

The first quotient represents the structure of the rock mass (Barton, 2002). This is useful for determining the difference between massive and fractured rock and serves as an approximate value for block volume.

The parameter  $J_n$  (Fig. 2-2) is determined by the number of joint sets



**Figure 2-3.** Examples for  $J_n$  values given as block diagrams and stereo nets (NGI, 2015).

seen in the rock mass (Fig. 2-3). Joints that only occur every several meters or that do not occur systematically are defined as random joints.

The second quotient represents the roughness and degree of alteration in the joint walls and serves as a measure of inter-block friction angle (Grimstad and Barton, 1998). This quotient can also be used to estimate the actual friction angle using equation (2-3) (Barton et al, 1973).

$$\tan^{-1}\left(\frac{J_r}{J_a}\right) \quad (2-3)$$

$J_r$  is based on the small scale and large scale roughness of the joint surface (Fig 2-4).

Small scale roughness (millimeters to centimeters) can be evaluated by running a finger along

a) Rock-wall contact		c) No rock-wall contact when sheared	
b) rock-wall contact before 10 cm shear		Zone containing clay mineral thick enough to prevent rock-wall contact	
Discontinuous joints	$J_r = 4$	Sandy, gravelly or crushed zone thick enough to prevent rock-wall contact	$J_r = 1$
Rough or irregular, undulating	3	Notes	
Smooth, undulating	2	i) Add 1 if the mean spacing of the relevant joint set is greater than 3-m	
Slickensided, undulating	1.5	ii) $J_r = 0.5$ can be used for planar, slickensided joints having lineations, provided the lineations are oriented for minimum strength	
Rough or irregular, planar	1.5		
Smooth, planar	1.0		
Slickensided, planar	0.5		
Note: i) Descriptions refer to small scale features and intermediate scale features in that order			

**Figure 2-4.** Chart for determining  $J_r$  value (Barton, 2006)

the joint wall. Large scale (order of decimeters to meters) roughness can be determined by laying a 1-m long ruler along the joint surface to determine the large scale roughness and amplitude (NGI, 2015). The least favorable value of  $J_r$  for the excavation should be used when determining  $Q$ . Infill also has an effect on the joint roughness value. If the infill is sufficiently thick that the joint walls will not make contact after 10 cm of shear then the roughness of the joint walls has no affect and  $J_r = 1$ .

$J_a$  is a parameter mainly concerned with the thickness and strength of joint fillings.  $J_a$  is affected by the thickness of the joint fill, type

of filling, and the degree of rock wall contact in the joint (Fig. 2-5). When clay is present in the joints it may be necessary to analyze the clay using laboratory test in order to establish the swelling properties of the clay (NGI, 2015).

The third quotient represents the active stresses happening in the rock mass (Barton, 1973).  $J_w$  is a measure of water pressure which has a negative effect on the shear strength of joints by reducing the effective normal stress and by possibly saturating clay layers within the joint (Fig. 2-6). SRF describes the relation between the rock's uniaxial compressive strength ( $\sigma_c$ )

Joint alteration number		$\phi_r$ approx	$J_a$
<b>a) Rock-wall contact (no mineral filling, only coatings)</b>			
A	Tightly healed, hard, non-softening, impermeable filling, i.e., quartz or epidote.	--	0.75
B	Unaltered joint walls, surface staining only	25-35°	1
C	Slightly altered joint walls. Non-softening mineral coatings, sandy particles, clay-free disintergrated rock, etc.	25-30°	2
D	Silty- or sandy-clay coating, small clay fraction (non-softening).	20-25°	3
E	Softening or low friction clay mineral coating, i.e. kaolinite or mica. Also Chlorite, talc, gypsum, graphite, etc., and small quantities of swelling clays	8-16°	4
<b>b) Rock-wall contact before 10 cm shear (thin mineral filling)</b>			
F	Sandy particles, clay-free disintergrated rock, etc.	25-30°	4
G	Strongly over-consolidated non-softening clay mineral fillings (continuous, but < 5 mm thickness)	16-24°	6
H	Medium or low over-consolidation, softening, clay mineral filling (continuous, but < 5 mm thickness)	12-16°	8
J	Swelling-clay fillings, i.e., montmorillonite (continuous, but < 5 mm thickness). Value of $J_a$ depends of percent of swelling clay-size particles, and access to water, etc.	6-12°	8-12
<b>c) No rock-wall contact when sheared (thick mineral fillings)</b>			
KL	Zones or bands of disintergrated or crushed rock and clay (see G, H, J for description of clay condition).	6-24°	6,8, or 8-12
N	Zones or bands of silty- or sandy-clay, small clay fraction (non-softening).	--	5
OP	Thick, continuous zones or bands of clay (see G, H, J for description of clay conditions)	6-24°	10, 13, or 13-20

**Figure 2-5.** Table for determining  $J_a$  values (Barton, 2002).

	Joint water reduction factor	Water $P_w$ $\approx$ (kg/cm <sup>2</sup> )	$J_w$
A	Dry excavations or minor inflow, i.e., < 5 l/m locally	<1	1
B	Medium inflow or pressure, occasional outwash of joint fillings.	1-2.5	0.66
C	Large inflow or high pressure in competent rock with unfilled joints.	2.5-10	0.5
D	Large inflow or high pressure, considerable outwash of joint fillings	2.5-10	0.33
E	Exceptionally high inflow or water pressure at blasting, decaying with time.	>10	0.2-0.1
F	Exceptionally high inflow or water pressure continuing without noticeable decay.	>10	0.1-0.05

**Figure 2-6.** Table for determining  $J_w$  values (Barton, 2002).

and major principle stress ( $\sigma_1$ ) (Fig. 2-7) (NGI, 2015). When possible SRF should be estimated by the ratio between  $\sigma_c$  and  $\sigma_1$  (Grimstad and Barton, 1993). If this is not possible, there are four different stress situations that help define SRF ratings: Weakness zones that intersect the underground opening which may or may not be able to transfer stresses in the surrounding rock mass, competent rock with stability problems due to high stresses or lack of stresses, squeezing rock with plastic deformation of incompetent rock under the influence of moderate or high rock stresses, and swelling rock (NGI, 2015).

A weakness zone is a zone that is substantially weaker than the surrounding rock (NGI, 2015). The width of this zone can range from 1 decimeter to multiple meters.

Weakness zones are commonly shear zones or areas with clay/ weak mineral layers.

Defining a rock mass as “squeezing rock” is appropriate when high rock stresses cause plastic deformation to take place (NGI, 2015). Swelling rock occurs when the rock contains minerals with swelling properties. In swelling rock laboratory test to determine the exact

Stress Reduction Factor			SRF	
<b>a) Weakness zones intersecting excavation, which may cause loosening of rock mass when tunnel is excavated</b>				
A	Multiple occurrences of weakness zones containing clay or chemically		10	
B	Single weakness zones containing clay or chemically disintergerated rock (depth of excavation $\leq$ 50 m).		5	
C	Single weakness zones containing clay or chemically disintergerated rock (depth of excavation $>$ 50 m).		2.5	
D	Multiple shear zones in competent rock (clay-free), loose surrounding rock (any depth)		7.5	
E	Single shear zones in competent rock (clay-free), (depth of excavation $\leq$		5	
F	Single shear zones in competent rock (clay-free), (depth of excavation $>$		2.5	
G	Loose, open joints, heavily jointed or "sugar cube", etc. (any depth).		5	
Notes: i) Reduce these values of SRF by 25-50% if the relevant shear zones only influence but do not intersect the excavation. This will also be relevant for characterization.				
<b>b) Competent rock, rock stress problems</b>				
	$\sigma_1/\sigma_3$	$\sigma_2/\sigma_3$	SRF	
H	Low stress, near surface, open joints.	$> 200$	$< 0.01$	2.5
J	Medium stress, favourable stress condition	200-10	0.01-	1
K	High stress, very tight structure. Usually favourable	10-5	0.3-0.4	0.5-2
L	Moderate slabbing after $>$ 1 hour in massive rock.	5-3	0.5-	5-50
M	Slabbing and rock burst after a few minutes in massive rock	3-2	0.65-1	50-200
N	Heavy rock burst (strain-burst) and immediate dynamic deformations in massive rock.	$< 2$	$> 1$	200-400
Notes: ii) For strongly anisotropic virgin stress field (if measured): When $5\sigma_1/\sigma_3 \leq 10$ , reduce $\sigma_1$ to $0.75 \sigma_1$ . When $\sigma_1/\sigma_3 > 10$ , reduce $\sigma_1$ to $0.5 \sigma_1$ , where $\sigma_1$ = unconfined compression strength, $\sigma_1$ and $\sigma_3$ are the major and minor principal stresses, and $\sigma_2$ = maximum tangential stress (estimated from elastic theory). iii) Few case records available where depth of crown below surface is less than span width. Suggest an SRF increase from 2.5 to 5 for such cases (see H). iv) Cases L, M, and N are usually most relevant for support design of deep tunnel excavation in hard massive rock masses, with RQD/J <sub>v</sub> ratios from about 50 to 200. v) For general characterization of rock masses distant from excavation influences, the use of SRF - 5, 2.5, 1, and 0.5 is recommended as depth increases from say 0-5 m, 5-25 m, 25-250 m, to $>$ 250 m. This will help to adjust Q for some of the effective stress effects, in combination with appropriate characterization values of J <sub>v</sub> . Correlations with depth - dependent static deformation modulus and seismic velocity will then follow the practice used when these were developed				
<b>c) Squeezing rock: plastic flow of incompetent rock under the influence of high rock pressure</b>				
		$\sigma_1/\sigma_3$	SRF	
O	Mild squeezing rock pressure	1-5	5-10	
P	Heavy squeezing rock pressure	$> 5$	10-20	
Notes: vi) Cases of squeezing rock may occur for depth $H > 350 Q^{1/3}$ according to Singh (1993) Rock mass compression strength can be estimated from $\sigma_{cm} = 5 \gamma Q_s^{1/3}$ (MPa) where $\gamma$ = rock density in t/m <sup>3</sup> , and $Q_s = Q^* \sigma_1/100$ .				
<b>d) Swelling rock: chemical swelling activity depending on pressure</b>			SRF	
R	Mild swelling rock pressure		5-10	
S	Heavy swelling rock pressure		10-15	

Figure 2-7. Table for finding SRF rating (Barton, 2002)

swelling properties of these minerals may be need to determine the SRF value (NGI, 2015).

### Geological Strength Index (GSI)

In order to provide a practical means to use the Hoek-Brown failure criterion the GSI rating system was created by Hoek et al. (2000). GSI is a qualitative rating system that ranges from 0- 100. The GSI chart was created by Hoek and Marinos (2000) for rating rock masses in the field (Fig. 2-8). Since GSI is a qualitative

measurement a higher variance can occur with different people rating the same rock mass. In order to mitigate this problem numerous attempts have been made to quantify the GSI rating (Somnez and Ulusay, 1999; Cai et al, 2004; Cai and Kaiser, 2006; Russo, 2007; Russo, 2009, Hoek et al, 2013). However, it should be noted that there are issues with trying to quantify the GSI system and that each one of these attempts has advantages and disadvantages (Hoek et al, 2013).

### Rock Mass Index (RMI)

RMI was developed by Palmström (1995) and is based on reduced rock strength caused

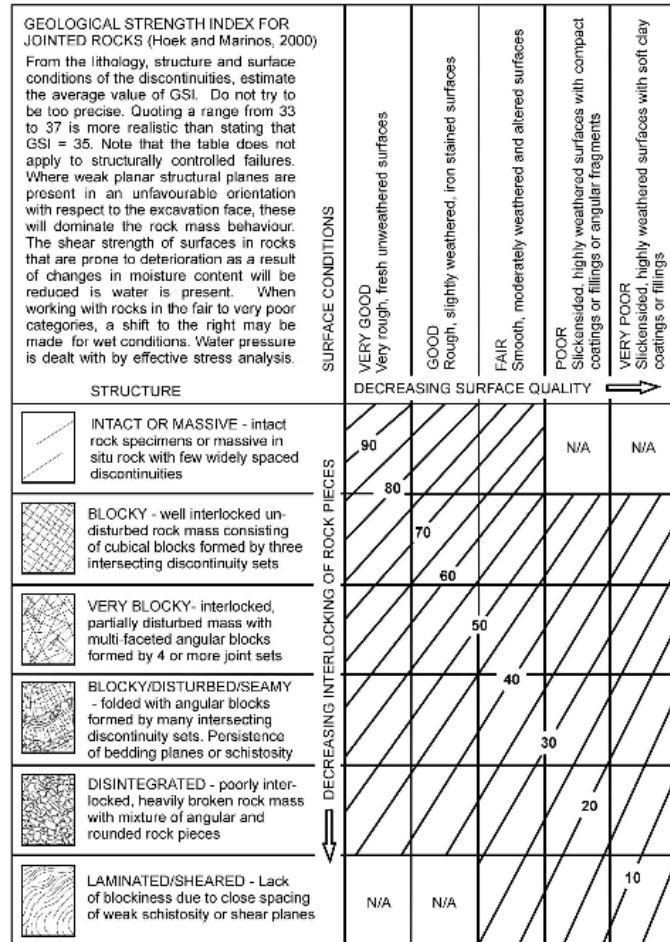


Figure 2-8. Basic structure of GSI chart (Hoek and Marinos, 2000).

by jointing. R<sub>Mi</sub> relies on two variable  $\sigma_c$  and JP:

$$R_{Mi} = \sigma_c * JP \quad (2-4)$$

JP is the jointing parameter of intact rock and is composed of the block volume, friction angle of block faces, length of joints, and continuity of joints:

$$JP = 0.2\sqrt{jC} * V_b^{D_{RMi}} \quad (2-5)$$

Here  $V_b$  is block volume and jC is joint condition factor. jC and D:

$$jC = jL * \frac{jR}{jA} \quad (2-6)$$

$$D_{RMi} = 0.37 * jC^{-0.2} \quad (2-7)$$

In the R<sub>Mi</sub> system the joint roughness factor (j<sub>R</sub>) is similar to the joint roughness factor found in the Q system. j<sub>R</sub> is based on the small scale (j<sub>s</sub>) and large scale roughness (j<sub>w</sub>) of the joint (EQ. 2-9). j<sub>s</sub> can be found by touch and values are given in figure 2-9. Large scale roughness can be calculated by dividing the maximum amplitude of

Term	Description	rating of J <sub>s</sub>
Very Rough	Near vertical steps and ridges occur with interlocking effect on the joint surface	3
Rough	Some ridge and side-angle steps are evident; asperities are clearly visible; discontinuity surface feels very abrasive (like sandpaper grade approx. < 30)	2
Slightly Rough	Asperities on the discontinuity surfaces are distinguishable and can be felt (like sandpaper grade approx. 30 -300)	1.5
Smooth	Surface appears smooth and feels so to the touch (smoother than sandpaper grade approx. 300)	1
Polished	Visual evidence of polishing exist, or very smooth surface as is often seen in coatings of chlorite and specially tals.	0.75
Slickensided	Polished and often striated surface that results from friction along a fault surface or other movement surface	0.6-1.5

The description is partly based on Bieniawski (1984) and Barton et al, (1974)

**Figure 2-9.** Descriptions for determining j<sub>s</sub> (Palmström, 1996).

Term for Waviness	Undulation	rating of j <sub>w</sub>
Interlocking (large scale)		3
Stepped		2.5
Large undulation	u > 3 %	2
Small - moderate undulation	u = 0.3 - 3 %	1.5
Planar	u < 0.3 %	1

**Figure 2-10.** Descriptions for visually determining j<sub>w</sub> (Palmström, 1996).

the joint by the measured length along the joint (EQ. 2-8). Due to this method being time consuming Palmström (1996) presents a table to determine j<sub>w</sub> using visual observations (Fig. 2-10). If the joint has a filling thick enough that there will be no rock wall contact when sheared j<sub>R</sub> = 1.

$$u = \frac{\text{Max amplitude}}{\text{Length of Joint}} \quad (2-8)$$

$$jR = j_s * j_w$$

(2-9)

The joint alteration factor  $j_A$

present in the RMi rating system is

also similar to the joint alteration

factor in the Q system (Fig. 2-11).

This factor represents the effects

the filling and coating material has

on the shear strength of joints. In the tables presented in figure 2-11 partial wall contact refers to a joint that will have rock wall contact within 10 mm of shear.

Joint length ( $j_L$ ) can be quantified by observing the discontinuity trace lengths on surface exposures. This leads to a crude estimation of joint length since discontinuities often persist farther than the observable rock mass. Palmström (1996) offers a formula to estimate the size range of joints:

$$jL = 1.5 * j_c * L^{-0.3} \tag{2-10}$$

Here L is the length of the joint in meters and  $j_c$  is 1 for continuous joints that terminate into

other joints and  $j_c$  is 2

for discontinuous joints

that terminate into

massive rock. Figure 2-

12 presents a list of

values for  $j_L$ .

A. Contact Between the Two Rock Wall Surfaces			
Term	Description	$j_A$	
<b>Clean joints</b>			
Healed or "welded" joints	Softening, impermeable filling (quartz, epidote, etc.)	0.75	
Fresh rock walls	No coating or filling on joint surface, except for staining	1	
<b>Alteration of joint wall</b>			
-1 grade more altered	The joint surface shows one class higher alteration than the rock	2	
-2 grades more altered	The joint surface shows two classes higher alteration than the rock	4	
<b>Coating or thin filling</b>			
Sand, silt, calcite, etc.	Coating of friction materials without clay	3	
Clay, chlorite, talc, etc.	Coating of softening and cohesive minerals	4	
B. Filled Joints With Partial or No Contact Between the Rock Wall Surfaces			
Type of Filling Material	Description	Partial wall contact thin fillings (< 5 mm) $j_A$	No wall contact thick filling or gouge $j_A$
Sand, silt, calcite, etc.	Filling of friction material without clay	4	8
Compacted clay materials	"Hard" filling of softening and cohesive materials	6	10
Soft clay materials	Medium to low over-consolidation of filling	8	12
Swelling clay materials	Filling material exhibits clear swelling properties	8-12	12-20

Figure 2-11. Tables for determining the joint alteration factor for RMi system.

Joint Length	Term	Type	$j_L$	
			continuous joints	discontinuous joints**
< 0.5 m	very short	bedding/foliation partings	3	6
0.1 - 1 m	short/small	joint	2	4
1 - 10 m	medium	joint	1	2
10 - 30 m	long/large	joint	0.75	1.5
> 30 m	very long/large (filled) joint, seam* or shear*		0.5	1

\*Often occurs as a single discontinuity, and should in these cases be treated separately.  
 \*\*Discontinuous joints end in massive rock

Figure 2-12. Tables for determining the joint length parameter for RMi (Palmström, 1996).

Block volume is related to the degree of jointing of the rock mass. Block volume is often

the most important parameter when determining RMI so great care should be taken when obtaining a block volume measurement. There is no set standard for measuring block volume and since blocks within a rock mass can often vary greatly in size block volume is not easily determined Palmström (1996) discusses multiple ways to quantify block volume but does not state that any one way of measuring block volume is preferable when evaluating RMI.

## **II. Approaches to Finding $E_{rm}$**

Empirical, analytical, numerical, laboratory test, and in situ methods have all been presented as solutions to find the answer to predicting  $E_{rm}$  but no clear answer has been found yet (Zhang, 2017).

There are a wide variety of empirical methods available in today's literature (Kayabasia and Gokceoglu, 2018; Zhang, 2017). Even though there are many different empirical methods all empirical methods relate the deformation modulus to a rock mass rating scheme such as RMR, Q, RMI, and GSI ratings. In addition to these ratings some methods include other variables such as disturbance factor, confining pressure, water quantity, elastic wave velocity, degree of anisotropy, modulus of the intact rock, and unconfined compressive strength (Zhang, 2017; Li et al., 2012; Saroglou and Tsiambaos, 2008; Hoek and Diederichs, 2006). Zhang (2017) tested a variety of empirical methods and found that the issue with these methods is that they are fitted with the case studies they are derived from and no single method could be proven to be more reliable than any other when applied outside of the data set they are derived from. Due to this, current research is stuck in a loop of providing new equations by verifying new equations based on their own unique dataset and claiming these new formulas are better than previously published formulas.

In situ and laboratory test are considered the most accurate way to measure  $E_{rm}$ . However, the methods are costly and time consuming and the accuracy of these test vary from one type of field test to another (Gage et al, 2014). They are also unable to accurately show the properties of the entire rock mass due a small sample size not being able to show all of the anisotropic features of a rock mass such as joints and fractures (Gage et al, 2014). Due to the location and budget constraints the most accurately known in situ methods may not be applicable to many projects.

*Numerical modeling has become more popular in recent years due to significant increases in computing power (JianPing et al, 2015). Numerical methods can be divided into two categories; finite element method (FEM) and discrete element method (DEM). While FEM modeling has been used, they have difficulty modeling the discontinuities present in a rock mass. Joint elements have been included in FEM in order to more accurately model the effect of discontinuities.*

## *Field Test*

### Plate Jacking Test

Plate jacking test are one of the most accurate in situ tests used in finding  $E_{rm}$  due to the relatively large volume of rock being tested (Fig. 2-13). Plate jacking test are normally only used in large budget projects such as dam construction due the cost of these experiments. A set of hydraulic jacks are used to apply a uniform load to a flat plate and the displacement is measured using extensometers embedded into the rock mass (Fig. 2-14). By using the extensometers, the



**Figure 2-13.** Plate jacking test (Rezaei et al, 2016).

effect the closing of fractures in the damage zone has on displacement values is reduced.

Knowing how much deformation occurs at a known

pressure makes it possible to calculate  $E_{rm}$ . This is typically done by using the International Society for Rock Mechanics (ISRM) suggested method (ISRM, 1979). This test can be performed in boreholes, shallow pits, or excavated underground test galleries (Fig. 2-13) (Boyle, 1992).

The common problems associated with plate jacking test are: condition of rock mass after site preparation, quality of measurement equipment, geometry of the test gallery, influence of discontinuities on stress distribution, different deformation mechanisms that may have an effect on the test depending on the orientation of discontinuities, and influence of the in-situ

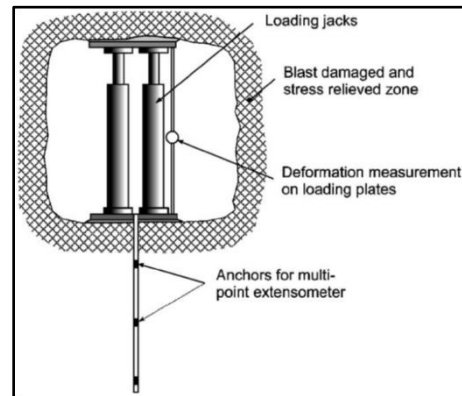


**Figure 2-14.** Diagram of plate jacking test and damage zones. (Hoek and Diederichs, 2006).

stress field (Agharazi et al, 2011). The damage zone around an excavation can lead to incorrect deformation values (Fig. 2-14). As the microfractures around the damage zone close a deformation value is given that does not accurately reflect the deformation of the intact rock.

While there is no way to fully prevent these microfracture from forming careful excavation of the testing site can help mitigate this problem and by measuring the displacement deep within the rock mass the effect of the microfractures are further limited. Developing new technology, such as fiber optic strain gauges, can also give us more accurate data than what was previously available (Gage, 2013). The other limiting factors listed must be taken into consideration when designing and interpreting the results from these experiments since there is no current method to reduce these sources of error (Agharazi et al, 2011). A plate loading test is similar to a plate

jacking test with the exception of the embedded extensometers used in a plate jacking test. In plate loading test the displacement is measured directly at the loading surface of the rock (Palmström and Singh, 2001). While being slightly cheaper, not using the extensometers leads to the damage zone having a greater effect on deformation measurements and thus results being less accurate.

### Borehole Test

There are three types of borehole test used: dilatometer, pressuremeter, and borehole jacking. Each method is suitable for testing different types of soil or rock (Fig. 2-15).

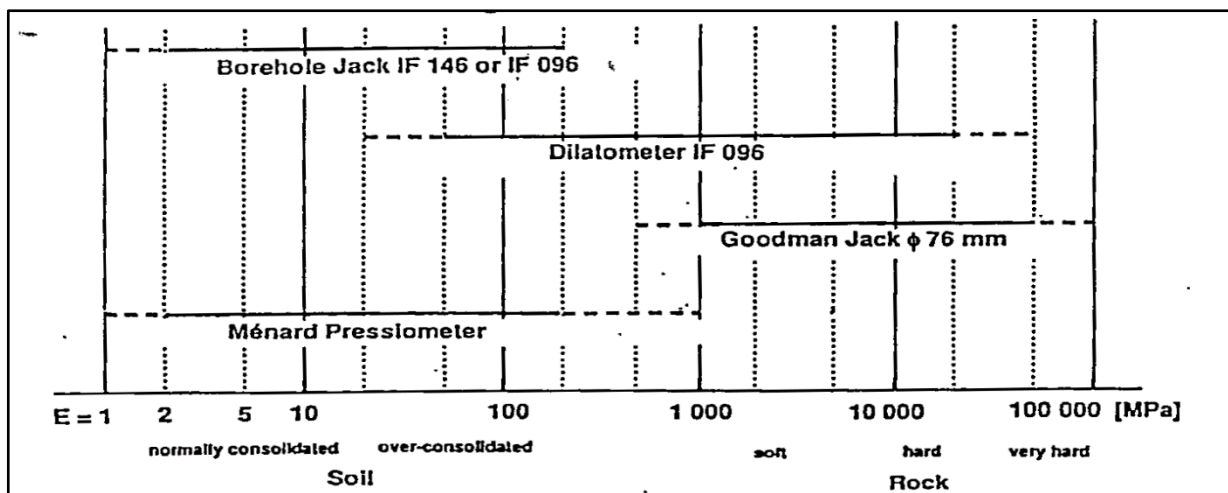


**Figure 2-15.** Application range of various types of borehole deformation probes (Sharma and Saxena, 2002).

A standard dilatometer test consists of creating a uniformly distributed pressure along the walls of a borehole via hydraulically expanding a membrane inside the borehole (Fig. 2-16). The displacement of the rock is measured by electric displacement gauges oriented in different radial directions. These gauges are oriented so that they can detect anisotropic behaviors in the tested ground. The measuring heads of the displacement gauges are located on the surface of the borehole or on the inside of the sleeve (Saxena and Sharma, 2002). By relating the change in the

borehole's diameter ( $\Delta d$ ), initial borehole diameter ( $d_i$ ), Poisson's ratio of the tested ground ( $\nu$ ), and change in effective dilatometer pressure ( $\Delta p_d$ ) it is possible to determine the modulus of the tested ground ( $E_{rm}$ ) using equation (2-11) (Saxena and Sharma, 2002).

$$E_m = (1 + \nu) * \frac{d_i}{\Delta d} * \Delta p_d \quad (2-11)$$

Pressuremeter (also called a Ménard Pressuremeter) test consist of a cylindrical probe with a flexible membrane that is used to apply uniform pressure to the walls of the borehole. This membrane consists of a main cell and two

guard cells (Fig. 2-17). The middle cell is filled with water and is expanded by either pumping in more fluid or gas. The guard cells are typically filled with gas and are kept at the same pressure as the main cell. The purpose of the guard cells is to prevent the main cell from expanding any direction other than radially (Ken, 2003). In

pressuremeter tests the expansion of the borehole is found by measuring the change in volume of the main cell (EQ. 2-12) (Saxena and Sharma, 2002; Ken, 2003). Unlike the dilatometer

$$E_m = 2 * (1 + \nu) * \frac{V}{\Delta V} * \Delta p_p \quad (2-12)$$

test a pressuremeter test will not detect anisotropic deformation. It will however, give an average modulus for a larger volume of rock

(Sharma and Saxena, 2002). Pressuremeter test are more suited for determining the modulus in

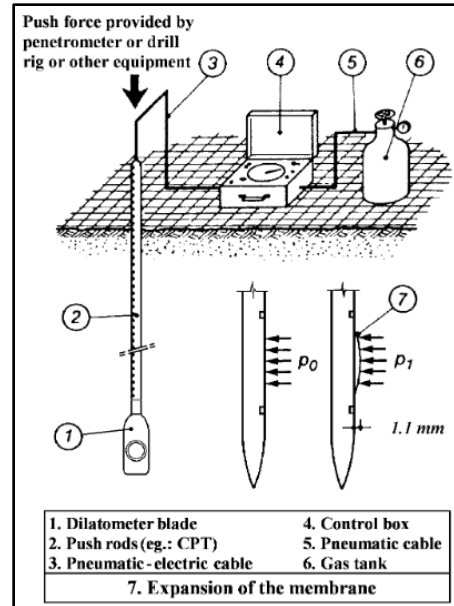


Figure 2-16. Dilatometer Test (Marchetti et al, 2001).

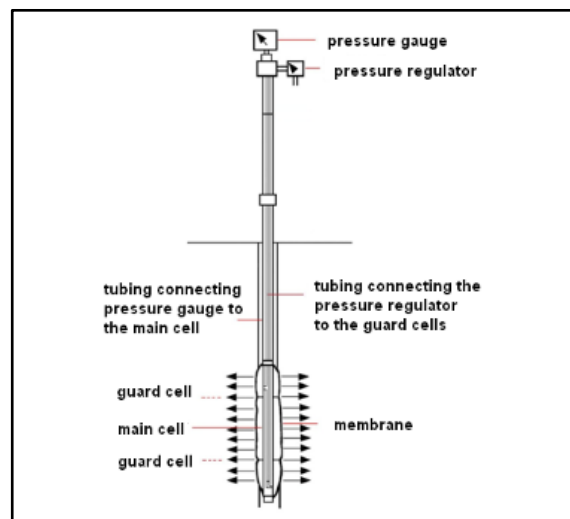


Figure 2-17. Sketch of a Ménard pressuremeter (Baguelin et al., 1972).

weak rocks and soils and should not be used for hard rocks (Fig. 2-15).

A Goodman jack test is another form of dilatometer test where unidirectional pressure is applied to the wall of the borehole by using two curved steel plates that are pushed apart by a hydraulic jack (Lo and Hefny, 2001). These tests are best for determining the modulus values for hard rock (Fig. 2-15). Like the dilatometer test electric displacement transducers are used to measure displacement in the borehole. These transducers measure how much the steel plates separate and if the plates tilt when load is applied. By using the separation of the load plates ( $\Delta h$ ), change in contact pressure over load plate area ( $\Delta p_j$ ), initial borehole diameter ( $d_i$ ), and an instrument correction factor ( $f$ ) (this depending on the angle of the load plates, load plate/borehole wall contact conditions, and  $\nu$ ) (EQ. 2-13) (Saxena and Sharma, 2002). A bore jacking test will affect about the same volume of rock that as a dilatometer test.

$$E_m = f * \frac{d_i}{\Delta h} * \Delta p_j \quad (2-13)$$

While borehole tests are easy and cost effective to perform the small volume of rock measured in these tests make their results less reliable than other in situ test. Borehole test also require carefully drilled holes and even the pressuremeter test, which is suitable for weak rocks and soil, can lead to less accurate results if the borehole is poorly drilled (Ken, 2003). There are also problems when trying to accurately determine the displacement of a Goodman jack's plates and, if the plates are allowed to tilt to much, damage can be caused to the instrument (Saxena and Sharma, 2002; Gage, 2014).



**Figure 2-18.** Flat jack to be inserted into rock mass (Hoek and Diederichs, 2006).

## Flat Jack Test

Flat jack tests are conducted by cutting a large slot into the rock mass and inserting a flat jack (Fig. 2-18) into the slot. The flat jack then applies pressure and the resulting deformation is measured. By using relationships between the pressure applied and the deformation caused it is possible to derive  $E_{rm}$ .

While flat jacking test are not as expensive as plate jacking test they still require a skilled drilling team and the flat jacks are not usually recoverable (Lo and Hefny, 2001). Results from flat jacking test are also subject to the same limitations as plate jacking test; closure in microfractures near the surface, deflection of plates, and closure between the plates and the rock mass cause inaccuracies in the displacement measurements (Hoek and Diederichs, 2006). However, the advantages of these tests are that you can test a larger volume of rock mass in a relatively non-disturbed zone of your excavation leading to more accurate modulus estimations than other test that use less rock volume.

## Pressure Tunnel and Radial Jacking Test

For a pressure tunnel test a section of circular tunnel is lined with waterproof material and sealed off by bulkheads. Next, water is pumped into the tunnel and the resulting rock deformation is measured.  $E_{rm}$  is then calculated using the elastic solution of a thick cylinder under internal pressure (Lo and Hefny, 2001).

A radial jacking test is performed by excavating a circular tunnel and applying evenly distributed radial pressure around the outside of the tunnel. The radial pressure is distributed by flat jacks positioned on a reaction frame.

While these tests are good in that they test a very large volume of rock to determine the

rock mass modulus they are also an incredibly expensive test. Due to the cost of these test only a few have been conducted (Hoek and Diederichs, 2006; Lo and Hefny, 2001).

#### Tunnel Relaxation Test

After a tunnel is excavated the deformation of the rock is measured. The rock mass modulus is then back calculated using the numerical analysis or relationships between the observed deformations and initial stresses (Lo and Lukajic, 1984).

This test leads to very reliable data since it uses field stresses and test a large volume of rock mass. However, since it involves tunnel excavation the test is very expensive compared to some of the other in-situ test listed here and not many have been performed.

#### Dynamic Test

These tests involve P and S wave velocities that are determined from a surface or downhole seismic method. Dynamic Young's modulus and dynamic shear modulus are determined through empirical relations between moduli, rock density, and P and S wave velocities (Lo and Hefny, 2001).

These tests are fast and inexpensive to perform. However, the value given from these tests are typically higher than the static parameters and represent the values at low stress and strain levels which is an inaccurate representation of most design stages (Lo and Hefny, 2001). These tests are also known to be less accurate than other in-situ test that directly deform the rock mass (Hoek and Diederichs, 2006).

## Stress Relief Test

For a stress relief test a vertical bore hole is drilled into the rock mass and the resulting diametric displacement is measured. This displacement is due to the in-situ test of the rock and the modulus is calculated from the displacements measured (Lo and Hefny, 2001).

This test is inexpensive and easy to perform but is limited to a relatively shallow depth. Due to the shallow depth and low volume of rock being measured the modulus values found from this test can be inaccurate.

## Numerical Modeling

### Finite Element Method (FEM)

FEM models are useful when calculating the forces occurring in irregular bodies. In order to find the force acting within the body said body is divided into simple geometric shapes called finite elements (Fig 2-19). Each of these finite elements has nodes. Nodes are always on the corners of each element and can also be placed in the middle of each side of the element (Fig 2-19). Nodes can move along the x, y, and z axis unless they are restrained by boundary conditions. Boundary conditions can restrict a nodes movement along single or multiple axis. Once the body is divided into elements, and the material properties and external loads are defined, the displacement of each node is expressed as a function in terms of its coordinates. Once this function for each node is found we can derive formulas for stress, strain energy,

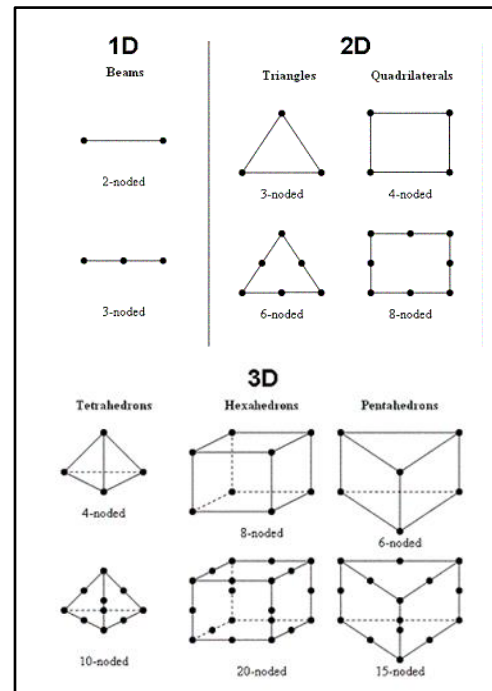


**Figure 2-19.** Types of elements for FEM (Moreno, 2011)

and potential energy of each nodes. A system of equations can now be used to define the complete element. The formulas for each node are then combined to create a solution for the entire body. This solution can be used to map the stresses across the body. The more nodes that are present in the body the more accurate the solution will be. In order to accurately model the rock mass, it is important to have a high density of nodes. However, as the number of nodes in our model increases so does computing time and results will not vary significantly once a sufficiently high density of nodes is created in the model.

FEM has been used to model jointed rock masses since the 1960's (Goodman et al, 1968). Since FEM is a continuum method it can have trouble when modeling highly fractured rock as it will not allow for the detachment of blocks which commonly occurs during failure (Hammah et al, 2008). However, with the addition of joint elements, which will split nodes along a joint element into two nodes on each side of the element. Closed joints (where the end of the joint is defined by a single node) are recommended when the joint element terminates into a bounded surface or intact rock. Open joints (where the end of the joint element is defined by two separate nodes that can move independently of each other) are recommended when the joint element terminates into a free surface or into another joint. With the addition of joint elements, FEM can now be applied to discontinuous rock masses and is still a commonly used tool for modeling discontinuous rock masses today (Hammah et al, 2008; Jian et al, 2016).

#### Discrete Element Method (DEM)

DEM models the rock mass as a discontinuum. Instead of dividing the body into simple geometric shapes the body is composed of multiple “particles” or discrete elements (Fig. 2-20). Each one of these particles has certain intact properties (UCS,  $E_i$ , etc.). The cohesive forces

between each of these particles can also be edited to reflect zones of weakness in the rock mass. Once this is done an external force is applied to the body and the force vectors for each particle are calculated. Once the force vectors on each particle is calculated stress and strain distributions throughout the body can be mapped out.

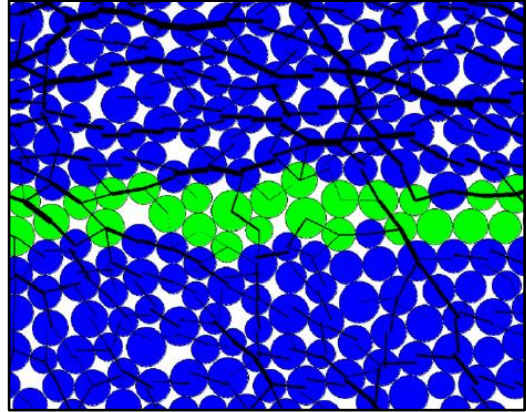


**Figure 2-20.** Representation of rock mass using DEM. Blue particles represent intact rock while green particles represent a joint (Ivars et al, 2011).

DEM is becoming increasingly popular in the field of rock mechanics due to its ability to accurately model joint and fracture geometry. Ivars et al. (2009) used DEM to construct a synthetic rock mass to simulate the behavior of jointed rock to obtain values for pre-peak and post-peak properties. The disadvantage to DEM is that it requires larger and more complex programs in order to be used when compared to FEM. These programs are often much more expensive and require a different knowledge base to operate.

## CHAPTER III METHODS

### I. Selection of Formulas

The empirical formulas for this study are chosen so that the effects of using different rock mass classification systems can be observed. Formulas with additional variables are also added in order to determine if the RMCS or if the addition of variables such as  $\sigma_c$  and  $E_i$  have a greater effect on  $E_{rm}$  predictions. Formulas are chosen based on the classification system used and their popularity in the literature. Each formula has a unique data set that it is derived from. As Zhang (2014) points out the accuracy of an empirical formula will be greater when applied to the data set it is derived compared the prediction of a formula derived from a different data set so it is important to test these empirical formulas with multiple data sets.

#### *Galera et al, 2005*

This study consists of relating the RMR of rock masses to the modulus of the intact rock determined by pressuremeter and dilatometer test. This formula (EQ. 3-1) is based on 702 data points where the  $E_{rm}$  from in situ test, RMR, and RQD are known (Table 3-1). In order to remove data that exhibits a “soil behavior” the authors excluded all data that had a weathering grade larger than IV or a pressuremeter/dilatometer modulus less than or equal to 0.5 GPa. Also, points were added to the RMR rating if  $E_{rm}$  was less than 10 GPa because a drained modulus was considered. The authors then performed a sensitivity analysis of the data using the following criterion: comparison of  $E_i$  vs.  $\sigma_c$ , comparison of  $E_i$

vs  $E_{rm}$ , and a comparison of  $E_{rm}/E_i$  vs RMR. After excluding the data with anomalous ratios the authors had a database consisting of 427 cases where  $E_{rm}$  and RMR are considered reliable, and 98 cases where  $E_{rm}$ ,  $E_i$ ,  $\sigma_c$ , and RMR are considered reliable.

Table 3-1. Galera et al (2005) data set.

Lithology	Number	Percent of Total Database
Igneous Rocks	270	38.5
Metamorphic Rocks	108	15.4
Detritic Sedimentary Rocks	175	24.9
Carbonate Rocks	101	14.4
Bibliography*	48	6.8

This formula was chosen for this test due to its use of RMR as a variable and that, in a study comparing 25 empirical formulas, Kayabasi and Gokceoglu (2018)

\*Includes data from Bieniawski, 1978; Serafim and Pereira, 1983; and Labrie et al, 2004.

found that this formula (3-1) had the highest predictive capabilities of all methods tested. This formula also allows us to see the effectiveness of combining  $E_i$  and RMR to predict  $E_{rm}$ .

$$E_{rm} = E_i * e^{\frac{(RMR-100)}{36}} \quad (3-1)$$

### *Barton, 2002*

This formula uses a normalized Q value presented in Barton (2002) and is derived from a data set made by combining Bieniawski (1978) and Serafim and Pereira (1983) (Table 3-2). This Q value is called  $Q_c$  and is related to the P-Wave velocity in rocks (EQ. 3-2).

$$Q_c = Q * \frac{\sigma_c}{100} \quad (3-2)$$

This new term  $Q_c$  is used when estimating the deformation modulus (EQ. 3-3). Barton argues that  $\sigma_c$  is easily measured and correlates strongly to Young's modulus and can improve the estimates of the deformation modulus. When comparing Barton's equation to existing formulas

that use RMR it was found that when  $Q < 1$  and  $RMR < 50$  the predictions for  $E_{rm}$  where the same. When  $Q > 1$  Barton's formula gave a conservative estimate unless  $\sigma_c > 100$ . This formula is shown to be able to give a wider range of modulus estimates than formulas that use RMR or GSI. The range for this formula is especially suited for trying to estimate the modulus in weaker rocks ( $RMR < 20$ ).

$$E_{rm} = 10 * Q_c^{\frac{1}{3}} \quad (3-3)$$

This formula was chosen due to the rarity of empirical relations between deformation modulus and Q rating. This formula is the most recent, and well known, attempt to relate Q rating and deformation modulus.

*Barton et al, 1983*

In order to find a relationship between the Q rating system and  $E_{rm}$  the author used in-situ test values for  $E_{rm}$  presented in Bieniawski (1978). Using this data set (Table 3-3) a formula for the  $E_{max}$ ,  $E_{min}$ , and  $E_{mean}$  based on the Q rating was found. This set of formulas was again tested against two independent set of in-situ test results in order to prove their validity (Voegelé et al,

Table 3-2. Barton (2002) data set.

Lithology	Number	Percent of Total Database
Massive	57	15.2
Amphibolite		
Granitic Gneiss	55	14.7
Diorite Gneiss	8	2.7
Massive Marble	2	0.5
Granite	4	1.1
Gneiss	32	8.5
Quartzite	36	9.6
Massive Gneiss	10	2.7
Quartzite Gneiss	163	43.5
Slate	8	2.1

1981; Bakhtar and Barton, 1983). In

Table 3-3. Barton (1983) data set.

both of these case studies the formal all gave reasonable values for  $E_{max}$ ,  $E_{min}$ , and  $E_{mean}$ .

Lithology	Number	Percent of Total Database
Massive Amphibolite	57	15.2
Granitic Gneiss	55	14.7
Diorite Gneiss	8	2.1
Massive Marble	2	0.5
Granite	4	1.1
Gneiss	32	8.5
Quartzite	36	9.6
Massive Gneiss	10	2.7
Quartzite Gneiss	163	43.5
Slate	8	2.1

The equation for  $E_{mean}$  was chosen for this study because it provided a second formula that uses the Q value to predict  $E_{rm}$ . When comparing formulas for predicting rock mass modulus the other two formulas presented in this paper are often ignored in favor of equation (EQ. 3-4). (Barton, 2002; Grimstad and Barton 1993) For the equation below  $E_{rm} = E_{mean}$ .

$$E_{mean} = 25 * \log(Q) \quad (3-4)$$

### *Beiki et al, 2010*

Using genetic programming the authors were able to create two formulas for the rock mass deformation modulus using GSI rating and UCS (EQ 3-5 and 3-6). 150 data points were

$$E_{rm} = \tan(\ln(GSI)) * \log(\sigma_c) * (RQD)^{\frac{1}{3}} \quad (3-5)$$

$$E_{rm} = \sqrt{\tan(1.56 + \ln(GSI))^2 * \sigma_c^{\frac{1}{3}}} \quad (3-6)$$

used to derive this formula with each data point including: elasticity of intact rock ( $E_i$ ), UCS ( $\sigma_c$ ), RQD, number of joints per meter (J/m), porosity (n), dry density, rock mass modulus via plate

loading test ( $E_{rm}$ ), and GSI rating. This data set covered a variety of lithologies (Table 3-4). All of the data was collected from boreholes at four dam sites in the Asmary Formation in Iran. In order to build the computer model, the database was divided into a training and a testing set. 40 randomly selected data points were reserved for the test set while the rest were used to train the model.

For this model the

Table 3-4. Beiki et al (2010) data set.

	Lithology	Number	Percent of Total Database
authors used the sum of the absolute error (SAE) between the measured modulus values found through flat jacking and the predicted values returned by each formula as a measure of fitness. After running the program through 50 generations with each generation having a population of 1,000 formulas	Shale, Sandstone – Quartzite, and Limestone	21	14.0
	Limestone	30	20.0
	Limestone and marl – Limestone with Silica Veins	56	37.3
	Sandstone, Siltstone, and Mudstone	43	28.7

the formula with the lowest SAE value was formula (EQ 3-5). Since RQD and GSI give information about the quality of the rock mass another formula without RQD (EQ 3-6) was created. Each formula was compared to previous formulas found in the literature that included RMR, GSI, D,  $E_i$ , and  $\sigma_c$ . When using the test data from this studies database it was found that the new formulas presented in this paper are the most accurate.

These formulas were chosen in order to have another GSI based formula to compare to the formula presented by Hoek and Diederichs (2006).

*Hoek and Diederichs, 2006*

This formula is based on the GSI rating and the disturbance factor for the rock mass. The database used to derive this formula is a set of 494 in situ test that cover a wide range of rock types (Table 3-5). The database includes  $E_{rm}$  found from the in-situ test (back analysis, flat jack, and plate test) and RMR and GSI ratings. Curve fitting software was used to fit a sigmoid function to this data set and equation 3-7 was derived.

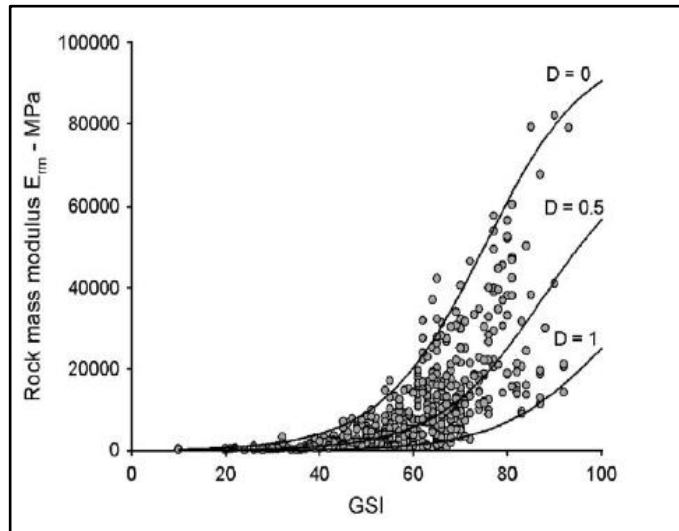


**Figure 3-1.** Plot of Hoek and Brown (2006) equation with in-situ data from China and Taiwan (Hoek and Diederichs, 2006).

$$E_{rm} = 100,000 \left( \frac{1 - \left(\frac{D}{2}\right)}{1 + e^{\frac{(75 + 25D - GSI)}{11}}} \right) \quad (3-7)$$

Hoek and Diederichs (2006) introduced a new variable called the disturbance factor (D). This factor ranges from 1 (fully disturbed) – 0 (undisturbed) and can help capture the full range of potential rock mass moduli (Fig. 3-1). This is a qualitative value and the guidelines for choosing this value can

be found in Hoek and Diederichs (2006). When the authors compared the formula to other measured field data they found that the  $D = 0$  curve gave a good fit for said data. In order to compare this formula to others that use RMR the prediction errors were compared (using  $D = 0.5$ ). The authors found that not only did their formula have a good fit to a data set that it was not derived from but that it had a reliably lower prediction error than other formulas that used RMR.

This formula was chosen because it is one of the most popular formulas for estimating  $E_{rm}$ . It is also the most popular formula that uses the GSI rating system.

*Palmström and Singh, 2001*

This formula was derived by fitting a curve to in-situ rock measurements from five different sources covering more than 50 different testing sites in India, Bhutan, and Nepal (Table 3-6).

Formula (3-8) (Palmström, 1995) was found to give values that are too low for  $E_{rm}$ . Formula (3-9) was found to give a better prediction of  $E_{rm}$  within the range  $1 < R_{mi} < 30$ .

$$E_{rm} = 5.6 * R_{mi}^{0.375} \quad (3-8)$$

$$E_{rm} = 7 * R_{mi}^{0.4} \quad (3-9)$$

These formulas were tested against two other prediction formulas that use RMR and Q

Table 3-5. Hoek and Diederichs (2006) data set.

Lithology	Number	Percent of Total Database
Sedimentary	260	52.6
Sandstone	117	23.7
Limestone	61	12.3
Siltstone	54	10.9
Silty-Shale	7	1.4
Claystone	2	0.4
Conglomerate – Mudstone	6	1.2
Mudstone	5	1.0
Shale	5	1.0
Sandy – Shale	3	0.6
Basalt	46	9.3
Migmatite	35	7.1
Agglomerate	30	6.1
Diorite	20	4.0
Granite	16	3.2
Dolerite	15	3.0
Andesite	11	2.2
Andesite – Tuff	5	1.0
Gabbro	1	0.2
Slate	26	5.3
Quartzite	10	2.0
Argillite	7	1.4
Chlorite	2	0.4
Gneiss	2	0.4
Schist	2	0.4
Metaconglomerate	6	1.2

rating systems. When compared to lab results involving massive rock masses equation (3-9) provided the most accurate predictions for  $E_{rm}$  although it still provided a value higher than the lab test results.

This set of formulas were chosen because they are the only published formulas that predict  $E_{rm}$  using RMI values. Palmström and Singh (2001) also argue that RMI gives a superior estimate of  $E_{rm}$  for massive rock than the Q and RMR system while being superior to Q and equal to RMR ratings when predicting  $E_{rm}$  for jointed rock.

*Read et al, 1999*

When looking at the predicted  $E_{rm}$  of a greywacke sandstone rock mass the authors found that formulas using GSI and RMR predicted values higher than the measured  $E_i$ . Noting that the deformation modulus of a rock mass should never be greater than the modulus of the intact material a new formula was proposed using in situ measurement from the greywacke sandstone.

$$E_{rm} = 0.1 * \left(\frac{RMR}{10}\right)^{0.3} \tag{3-10}$$

This formula provided reasonable values when tested against the data set available to the authors (Table 3-6) where other formulas would yield impossible answers.

Table 3-6. Read et al, (1999) data set

Lithology	Number	Percent of Total Database
Sandstone	21	70
Mudstone	9	30

This formula was chosen as a second RMR formula because when tested against other formulas that used exclusively RMR rating it was found to be the most accurate (Shen et al, 2012).

## II. Building and Validating the Numerical Models

Using RS2 (formerly RS<sup>2</sup> or Phase<sup>2</sup>) finite element software 24 numerical models of transversely isotropic rock masses are constructed. These models are built using four sets of joint and material properties derived based on assigning realistic combinations of values to RMR parameters that create four different rock mass conditions corresponding to selected RMR values of 30, 45, 60, and 75. Different orientations of transverse isotropy are created for each rock mass condition by introducing parallel and continuous sets of joints at six selected angles from the ground surface; 0°, 30°, 45°, 60°, 75°, and 90°. The naming convention adopted for the models is RMR(RMR value)\_(angle of joints relative to ground surface). Where a model is referred to without listing the joint angles then the statement applies to all models with that rating regardless of joint orientation.

RMR system is chosen over the other three RMCS used in this study because the variables of RMR are easier to define and RMR is more widely used in practice. Well defined variables allow models to be built more consistently as our estimates are better constrained. RMR system covers nearly all of variables that constitute the Q, RMI, and GSI systems along with a few additional parameters (Table 3-7). The four selected RMR values represent a wide range of rock mass conditions/qualities from poor to good rock masses.

Values of those input parameters that are needed to build the numerical models that are not part of the RMR system are estimated with reference to the rock types defined by taking the UCS (uniaxial compressive strength) range as a reference. For example, our RMR75 model has a UCS of 110 MPa which falls within the UCS range of sandstone; any variable that is not given by the RMR system is assigned a value that would be appropriate for that sandstone.

In the following, the process of building and validating the empirical models is discussed

along with the methods of testing the empirical equations. First, the common characteristics between all of the numerical models is described. Second, the unique characteristics of each model is covered. Next, we discuss the methods used to show that the results from these models are a valid representation of a real rock mass. Finally, the methods used to determine the effectiveness of the selected predictive formulas discussed previously are covered.

Table 3-7. Variables accounted for in each RMCS.

RMCS	Variables											V <sub>b</sub>
	UCS	Spacing of Joints	Joint Length	Aperture	Joint Roughness	Infilling	Weathering	Water Conditions	Joint Orientation	RQD	Number of Joint sets	
RMR	✓	✓	✓	✓	✓	✓	✓	✓	✓	✓		
GSI		✓					✓					
Q		✓		✓	✓	✓	✓	✓	✓	✓	✓	
RMi	✓	✓	✓	✓	✓	✓	✓					✓

Table 3-8. RMR ratings for each model.

Models		UCS (MPa)	Spacing Of Joints (m)	Joint Length (m)	Joint Aperture (mm)	Roughness	Infilling	Weathering	Groundwater Conditions	Orientation Of Joints	RQD
RMR30	Value	45	0.05	11	6	Slightly Rough	Soft Filling	Highly Weathered	Dry	Favorable	24
	RMR Rating	4	5	1	0	3	0	1	15	-2	3
RMR45	Value	70	0.5	11	6	Slightly Rough	Soft Filling	Moderately Weathered	Dry	Favorable	35
	RMR Rating	7	10	1	0	3	0	3	15	-2	8
RMR60	Value	120	0.5	11	3	Slightly Rough	Soft filling	Slightly Weathered	Dry	Favorable	70
	RMR Rating	12	10	1	1	3	2	5	15	-2	13
RMR75	Value	110	0.5	11	0	Smooth	None	None	Dry	Favorable	91
	RMR Rating	12	10	1	6	1	6	6	15	-2	20

### Common characteristics between models

A distributed (line) load of 10 MPa is placed in the middle of the model to simulate a bridge footing on the top surface of the rock mass. The size of each model is 10 m x 6 m in order to avoid boundary effects on the

pressure bulb created by the stresses caused by the applied load. Boundary conditions are set to be unrestrained on the top surface, restrained on the x axis along the right and left edges, and restrained on the x and y axis along the bottom surface (Fig. 3-2). These

boundary conditions correspond to a

rock mass domain away from the influence of free surfaces. A 3 node triangular element mesh type is chosen to discretize the models. The models are discretized with increasingly finer mesh size (increasing node density) as the discontinuity spacing decreases.

The failure criterion for the intact rock is selected to be the Mohr-Coulomb criterion. To define Mohr-Coulomb values (friction angle and cohesion) RocData software is used. In RocData it is possible to derive a rock's friction angle ( $\phi$ ), cohesion value (C), and intact elastic modulus ( $E_i$ ) from a UCS, GSI,  $m_i$ , D, and MR variables. These values are easily found using our current RMR data. GSI is found from using equation 3-11 (Bieniawski, 1989):

$$GSI = RMR - 5 \quad (3-11)$$

The  $m_i$  and MR variables are dependent on the lithology of the rock. The UCS for every model is in the range of sandstone with the exception of the RMR30 models (to be explained later).

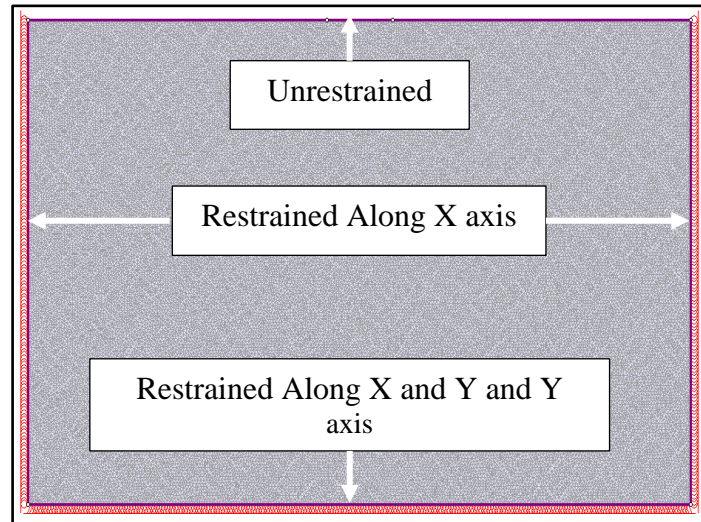


Figure 3-2. Model with boundary conditions.

Therefore,  $m_i$  and  $M_R$  values are based on sandstone for RMR45, RMR 60, and RMR 75 models. Unit weight, poisson's ratio, and porosity are also based on the assumed lithology of the models. Disturbance factor ( $D$ ) is considered to be 0 since the surface loading does not involve excavation. The peak values for the Mohr-Coulomb failure criteria ( $\phi_p$  and  $C_p$ ) are found by using values derived from the RMR ratings. Residual values ( $\phi_r$  and  $C_r$ ) are found by calculating the residual GSI values ( $GSI_r$ ) using the methods presented in Cai et al. (2004).

When defining the joint properties, the Barton-Bandis shear strength criterion is used. Joint compressive strength (JCS) is found by reducing the UCS listed in the initial RMR rating by a factor that is dependent on the weathering at the joint surface (Hack and Price, 1997), JRC is found based on each model's RMR rating, and the friction angle is based on the joint filling properties.

All models converge and yield a stable solution at a tolerance value below 0.004. Every model presented in this study is able to converge with a tolerance at or below this threshold within 1000 iterations.

Model	JCS (MPa)	JRC	$\phi_{ij}$ (deg)	$K_n$ (MPa/m)	$K_s$ (MPa/m)
RMR30	15.75	2	22.0	2000	600
RMR45	49.00	2	22.0	2000	600
RMR60	106.00	4	22.0	2000	800
RMR75	110.00	2	26.8	37200	18600

### *RMR30 Models*

Any movement along the joints is facilitated by the filling material in the joint. Due to this the joint roughness coefficient (JRC) and the residual friction angle ( $\phi_{rj}$ ) are both based on the infill. Normal and shear stiffness ( $K_n$  and  $K_s$ ) of the joints are based off of values for the stiffness of clay filled joints as suggested by Barton (2006). The joint properties for the RMR30 model can be found in Table 3-9. The intact properties of this model that cannot be found in the

RMR system are based on values that are reasonable for siltstone. Siltstone is chosen because the UCS used to determine the RMR value falls within the expected range of UCS in siltstone. The material properties of the RMR30 models can be found in Table 3-10. Due to the low strength values of the model the distributed load was reduced to 5 MPa in order to every element in the model from yielding and to have a converging solution.

### *RMR45 Models*

When constructing the RMR45 models much of the same variables used in the RMR30 models are used with the main difference being in the UCS and the weathering values (Table 3-8). The increase in UCS led to parameters that are not defined by the RMR values to be assumed using reasonable parameters for sandstone. This change in assumed lithology between models should not matter for the purposes of this test due to the fact that the empirical relations being tested are presumably valid for any lithology. Since these models are constructed to simulate real rock masses the differences in presumed lithology should not matter as long as all of the characteristics defined within the models can reasonably exist within the assigned lithology. Due to the UCS and weathering characteristics changing, the JCS values for the joints in the RMR45 model were increased in accordance to Hack and Price (1997) while all other joint characteristics remained the same due to the identical infilling properties (Table 3-9). The material properties of the RMR45 models can be found in Table 3-10.

### *RMR60 Models*

Once again, the UCS of the intact rock is increased (Table 3-8). This new value still falls within the potential range of UCS for sandstone so once again acceptable values for sandstone

are used to determine any variables for the model not explicitly defined in the RMR rating. Additionally, the amount of infilling decreases in this rock mass. To reflect this decrease  $K_s$  is increased for the RMR60 models according the upper end of possible values for stiffness of clay filled joints published by Barton (2006). The JRC is also increased slightly to reflect the smaller amount of infilling in the joints leading to a higher potential for rock wall contact (Table 3-9). The material properties of the RMR60 models can be found in Table 3-10.

### *RMR75 Models*

The most significant change in the RMR 75 models is that the joints in the model no longer have infilling. All movement along these joints is governed by the properties of the rock walls of the joints. Using Barton (2006) it is possible to assign appropriate  $K_n$  and  $K_s$  ratings according to measurements of jointed sandstone (Table 3-9). Residual friction angle of the joint ( $\phi_{ij}$ ) is based on the residual friction angle ( $\phi_r$ ) found for the intact rock (Table 3-8). The material properties of the RMR75 models can be found in Table 3-10.

### *Model Validation*

In order to determine if the numerical models built are viable the results are compared with equations 3-12 – 3-14 for stress distribution in a transversely isotropic rock mass (Goodman, 1989).

$$\sigma_r = \frac{h}{\pi r} \left( \frac{X \cos(\beta) + Y g \sin(\beta)}{(\cos^2(\beta) - g \sin^2(\beta))^2 + h^2 \sin^2(\beta) \cos^2(\beta)} \right) \quad (3-12)$$

$$g = \sqrt{1 + \frac{E_i}{(1-\nu^2)K_n S}} \quad (3-13)$$

$$h = \sqrt{\frac{E_i}{1-\nu^2} \left( \frac{2(1+\nu)}{E} + \frac{1}{K_s S} \right) + 2 \left( g - \frac{\nu}{1-\nu} \right)} \quad (3-14)$$

The parameters  $g$  and  $h$  given by Equations 3-13 and 3-14 are functions of the intact properties of the rock [modulus of elasticity ( $E_i$ ), poisson's ratio ( $\nu$ )] and the joints ( $K_n$ ,  $K_s$ , and joint spacing ( $S$ ]). Equation 3-12 is used to map the stress through the rock mass. This formula uses the distance from the point load application ( $r$ ), component of

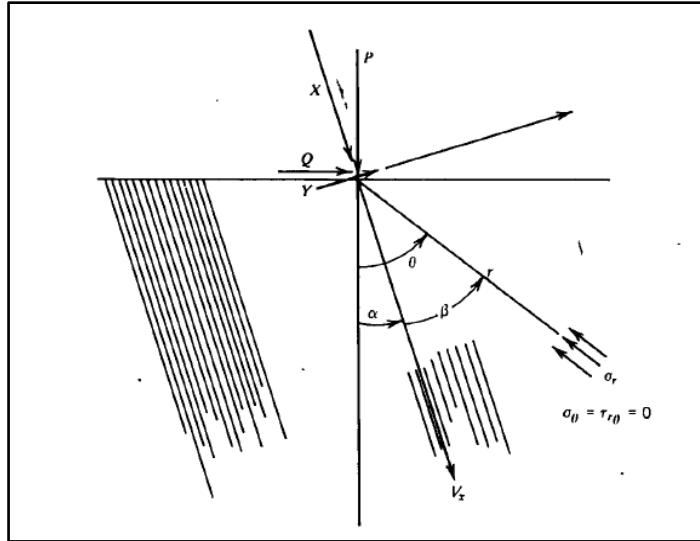


**Figure 3-3.** Diagram of  $X$ ,  $Y$ ,  $\alpha$ ,  $\beta$ , and  $\theta$  for equation 2 (Goodman, 1989).

the load that is parallel to the planes on anisotropy ( $X$ ) and component of the load that is perpendicular to the planes of anisotropy ( $Y$ ) (both of these values are always positive).  $\beta$  can be found by  $\beta = \theta - \alpha$  (Fig. 3-3). This solution is originally developed for a point load by John Bray, however experiments by Gaziev and Erkliham (1971) show that the formula can also predict stresses caused by distributed loads (Goodman, 1989).

Using the plotting software MATLAB, 2,581 points (Fig 3-4) are plotted to make a contour map of stresses in an isotropic rock mass with the same properties as those of the numerical models built in RS2. If these

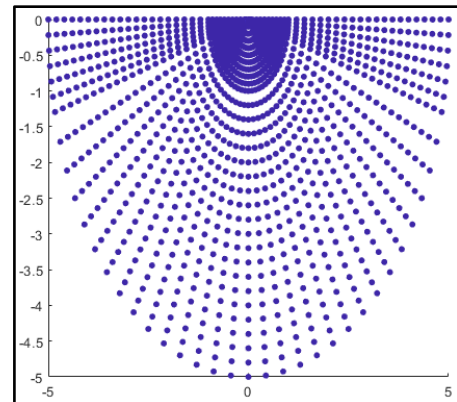


**Figure 3-4.** Mapped points used for contours in analytical solution.

stress distributions from our numerical models match the stress distributions given by the analytical models we can verify that our numerical models are behaving like real rock masses. The stress distribution is compared between models that have the same discontinuity orientations as the solutions given by Goodman (1989). Therefore, the models with a discontinuity

orientation of 75 degrees is not compared to the analytical method.

### III. Testing the Formulas

Our 24 numerical models are originally built using the RMR system. Based on the parameter values for each of the selected RMR ratings (30, 45, 60 and 75), equivalent ratings for Q and R<sub>Mi</sub> are derived

Table 3-12. RMCS value for each model.

	RMR	Q	GSI	R <sub>Mi</sub>
RMR30	30	0.36	25	0.3
RMR45	45	1.20	40	10.5
RMR60	60	1.80	55	20.2
RMR75	75	12.10	70	37.2

(Table 3-12) (Fig. 3-5) while the GSI values are predicted directly from Equation 1 since the GSI values cannot be derived directly from RMR parameters. The derived values of Q and R<sub>Mi</sub> ratings are then verified using the pairwise correlations with the selected RMR ratings (Table 3-11). The vertical stress and total displacement distributions computed for the numerical models are taken as realistic responses of the different rock masses represented by the four RMR ratings. These models are considered as the references to evaluate the performances of the predictive formulas. Stresses will be mapped out along the centerline and surface of each model (Fig. 3-6).

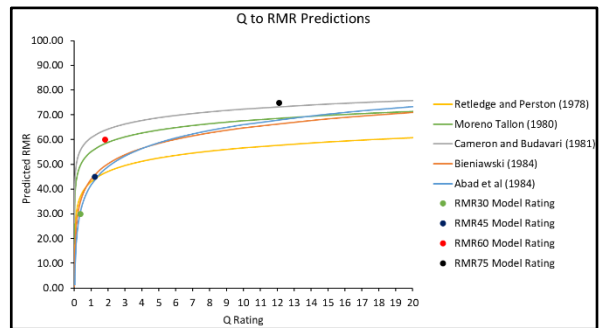


Figure 3-5. Empirical relations between Q and RMR rating along with Q and RMR values from Table 6.

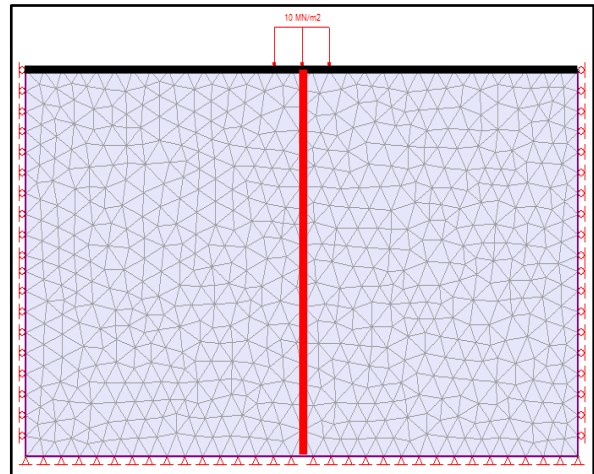


Figure 3-6. Total deformations will be mapped out along the center line of the model (red line) and along the surface (black line).

Once we have the rating for each model using all four of the RMCS the predicted  $E_{rm}$  from each equation is found (Table 3-13). Isotropic FEMs are made with the same intact properties as the transversely isotropic RMR30, RMR45, RMR60, and RMR 75 models. However, there will be no joint systems placed in these models and the  $E_i$  value used in the models will be changed to the  $E_{rm}$  values given by the predictive formulas (Table 3-13). With all of the variables being the same with the exception of the elastic modulus we can see how well each formula defines the deformations of the rock masses. Deformations along the top surface of the models and along a center line running through the middle of the distributed load will be graphed. These predicted deformations and the actual deformations given by each of our 24 RMR model will be compared.

Table 3-13. Predictive formula results.

RMCS	Predictive Formula	Predicted $E_{rm}$ For Models (GPa)			
		RMR30	RMR45	RMR60	RMR75
RMR	Read et al, 1999	2.7	9.1	21.6	42.2
	Galera et al, 2005	2.3	4.2	10.9	15.1
Q	Barton et al, 1983	2.0	6.1	6.1	27.1
	Barton, 2002	8.1	10.7	12.8	23.7
GSI	Hoek and Diedrichs, 2006	7.9	14.0	38.8	71.3
	Beiki et al, 2010	5.9	6.1	8.7	16.4
RMi	Palstrom and Singh, 2001	3.8	17.9	23.3	n/a

Table 3-10. Properties of intact rock not given by RMR.

Model	Unit Weight (MN/m <sup>3</sup> )	Poisson's Ratio	Young's Modulus (E <sub>i</sub> ) (MPa)	Peak Tensile Strength (MPa)	Peak Cohesion (C <sub>p</sub> ) (MPa)	Peak Friction Angle (φ <sub>p</sub> ) (Deg.)	Residual Tensile Strength (MPa)	Residual Friction Angle (φ <sub>r</sub> ) (MPa)	Residual Cohesion (C <sub>p</sub> ) (MPa)	Dilation Angle (Deg.)	Porosity (n) (%)	Residual GSI
RMR30	0.026	0.19	15750	0	1.600	24.689	0	0.663	14.660	0	0.02	5
RMR45	0.023	0.13	19250	0	3.528	32.058	0	20.139	1.137	0	0.02	5
RMR60	0.023	0.13	33000	0	7.500	36.600	0	20.139	2.258	0	0.10	5
RMR75	0.026	0.13	30250	0	8.714	41.029	0	26.800	4.025	0	0.10	23

Table 3-11. Predictive relations between RMCS

Publication	Q to RMR Predictions	RMi to RMR Predictions	Q to RMi predictions	RMR to GSI predictions
Bieniawski (1984)	$RMR = 9 * \ln(Q) + 44$			
Rutledge and Perston (1978)	$RMR = 5.9 * \ln(Q) + 43$			
Clarke and Budavari (1981)	$RMR = 5 * \ln(Q) + 60.8$			
Abad et al, (1984)	$RMR = 5.4 * \ln(Q) + 41.8$			
Barton (1995)	$RMR = 15 * \log(Q) + 50$			
Kumar et al, (2004)		$RMR = 5.4 * \ln(RMi) + 54.4$	$RMi = 0.5 * Q^{0.93}$	
Hashemi et al, (2009)		$RMR = 7.5 * RMi + 36.8$	$RMi = 1.082 * Q^{0.4945}$	
Bieniawski (1989)				$GSI = RMR - 5$

## CHAPTER IV RESULTS

In this section the results of numerical simulations for the four main rock mass conditions, validation of the numerical models, and the mapped deformations from each model (RMR30, RMR45, RMR60, RMR75) along with the predicted mapped deformations is discussed.

### I. Analytical vs Numerical Stress Patterns

The left column in Figure 1 shows the stress patterns from the analytical solution (4-12). The contours represent 1 MPa stress increments from 1 – 18 MPa. Where the outermost contour is the largest complete contour within the model domain. The stress distributions numerically computed for the RMR75 model set are presented on the right column whereas the results for the other angles can be found in Appendix A.

### II. $E_{rm}$ Predictions

Table 1 shows the predicted  $E_{rm}$  values for each of the four rock mass conditions using the selected empirical formulas. Figures 2-9 show the total deformations of RMR30, RMR45, RMR60, and RMR75 along with the predicted deformations found by each formula. RMR30 models do not show the displacements with a 90° orientation due to the model not being able to converge. RMR45 and RMR60 models showed maximum displacement curves when the orientation of discontinuities 30° from the surface and minimum displacement curves when discontinuities are 90° from the surface(Figs. 4 - 7). These observations do not hold in the RMR30 or RMR75 models(Figs. 1,2,8, and 9)

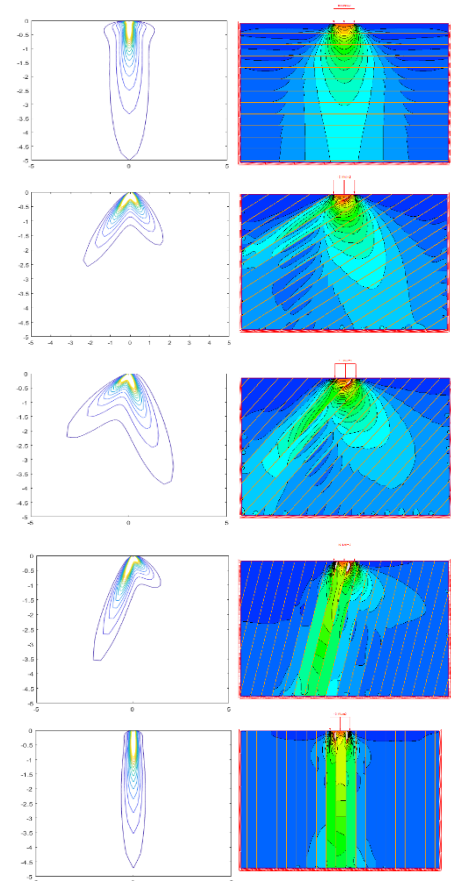
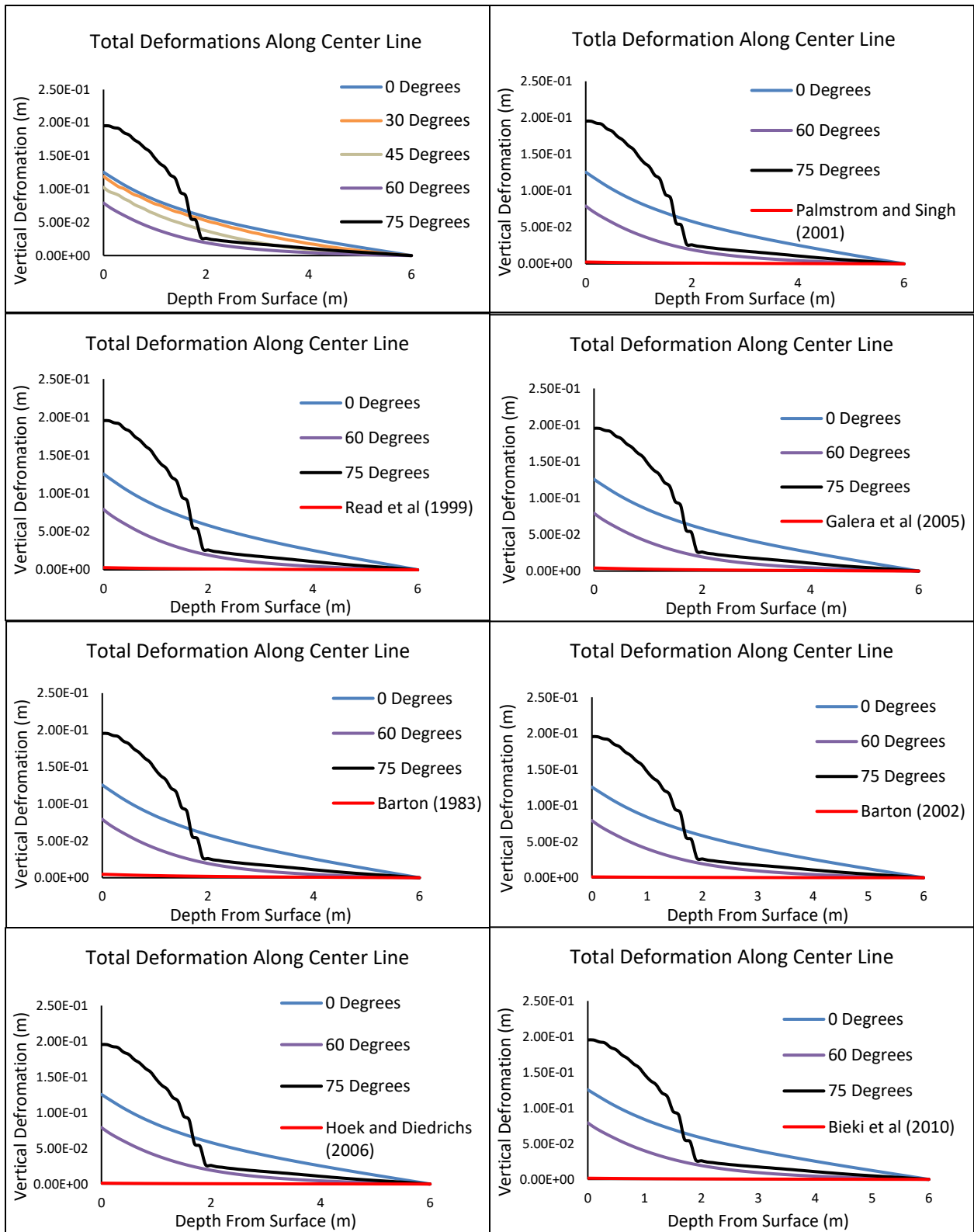


**Figure 4-1.** Comparison of analytical (left) and numerical (right) vertical stress distribution for models with discontinuities tilted 0°, 30°, 45°, 60°, and 90° from the surface (ordered from bottom to top).

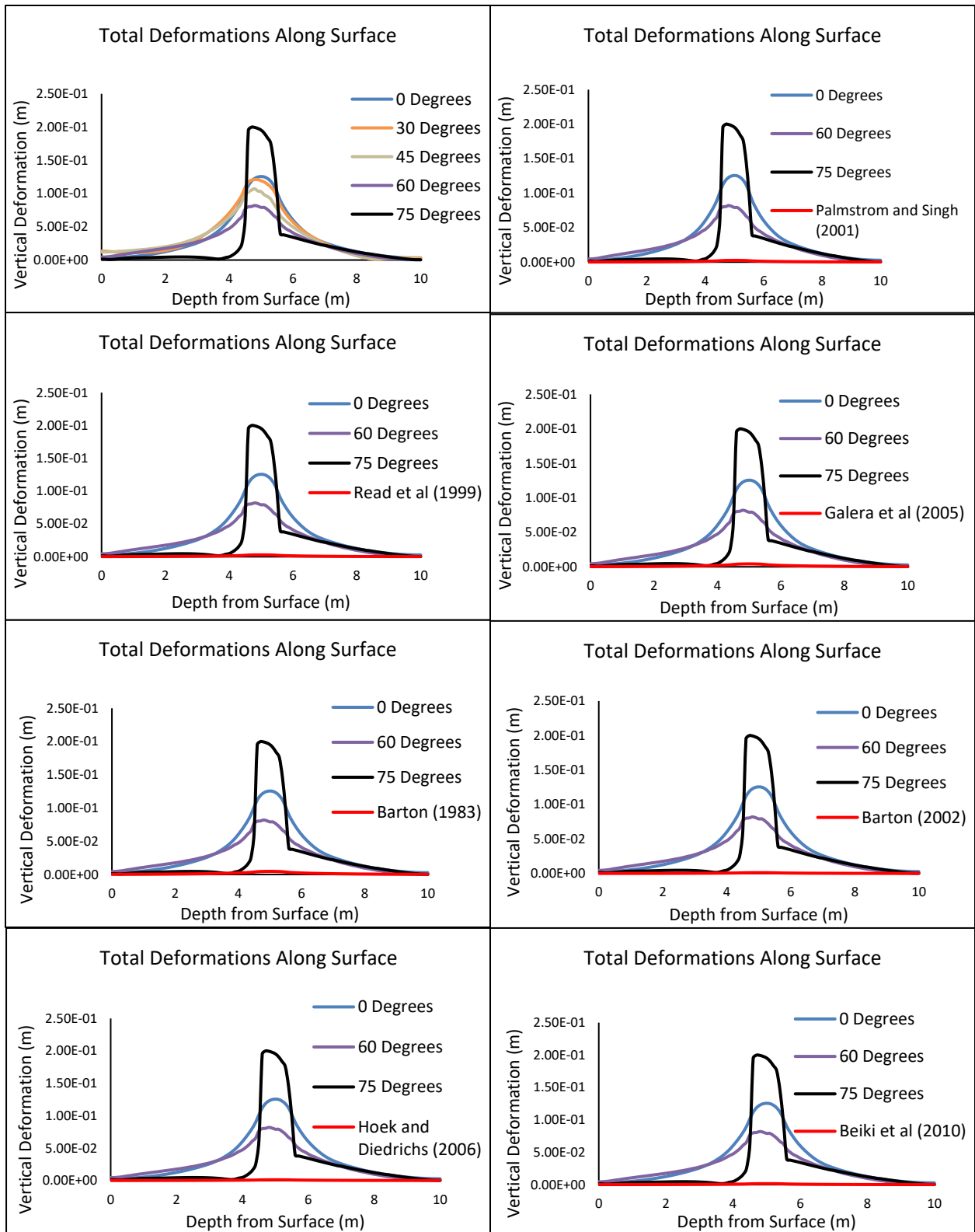
Across all models predictive formulas predicted deformations either in the lower range or well below the numerically computed deformation range. The RMR30 models show that none of the predictive formulas come close to predicting the deformations seen in the numerical models (Figs. 2 and 3). In the RMR45 models, Galera et al (2005) is the only predictive formula to predict deformations within the possible range of displacements while every other formula underpredicts the deformations. The Barton (1983) and Bieki et al (2010) formulas predict identical curves for the RMR45 models. When looking at the RMR60 models, Bieki et al (2010) and Barton (1983) are the only predictive equations that fall within the lower range of possible deformations (Figs. 6 and 7). Galera et al (2005) and Barton (2002) both predict similar deformation curves in these models but both are just below the minimum predicted deformations. In the RMR 75 models Galera et al (2005) and Bieki et al (2010) now offer the best predictive equations but they still only predict the lower end of the possible deformations (Figs 8 and 9).

Table 4-1. Predictive formula results

RMCS	Predictive Formula	Predicted $E_m$ For Models (GPa)			
		RMR30	RMR45	RMR60	RMR75
RMR	Read et al, 1999	2.7	9.1	21.6	42.2
	Galera et al, 2005	2.3	4.2	10.9	15.1
Q	Barton et al, 1983	2.0	6.1	6.1	27.1
	Barton, 2002	8.1	10.7	12.8	23.7
GSI	Hoek and Diedrichs, 2006	7.9	14.0	38.8	71.3
	Beiki et al, 2010	5.9	6.1	8.7	16.4
RMi	Palmström and Singh, 2001	3.8	17.9	23.3	n/a



**Figure 4-2.** Maximum and minimum total deformations along the center line of the distributed load of each numerical model of RMR30 rock mass along with predicted deformations by the selected empirical formulas Table (1-1).



**Figure 4-3.** Maximum and minimum total deformations along the surface of each numerical model of RMR30 rock mass along with the predicted deformations by the selected empirical formulas Table (1-1).

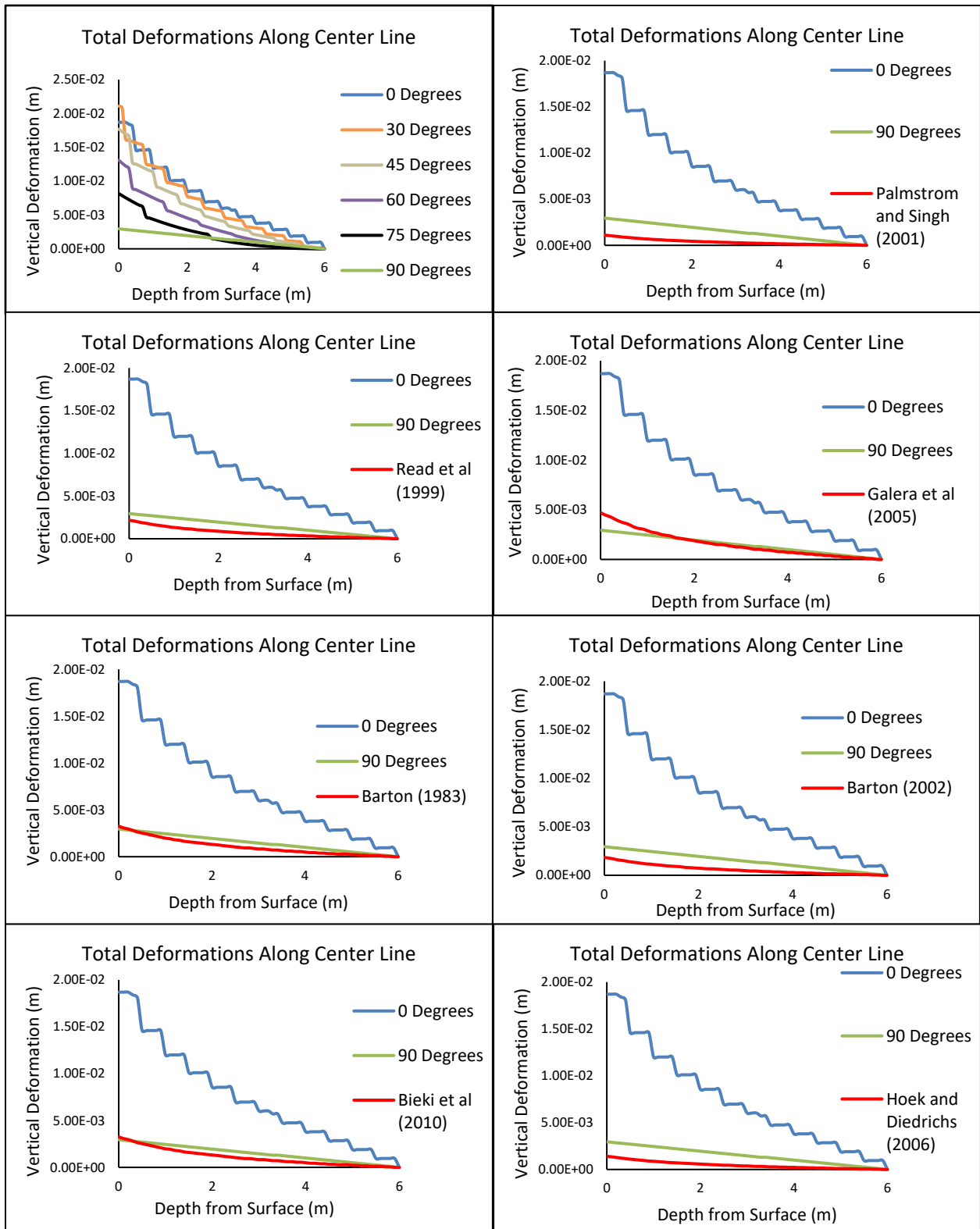


**Figure 4-4.** Maximum and minimum total deformations along the center line of the distributed load of each numerical model of RMR45 rock mass along with predicted deformations by the selected empirical formulas Table (1-1).

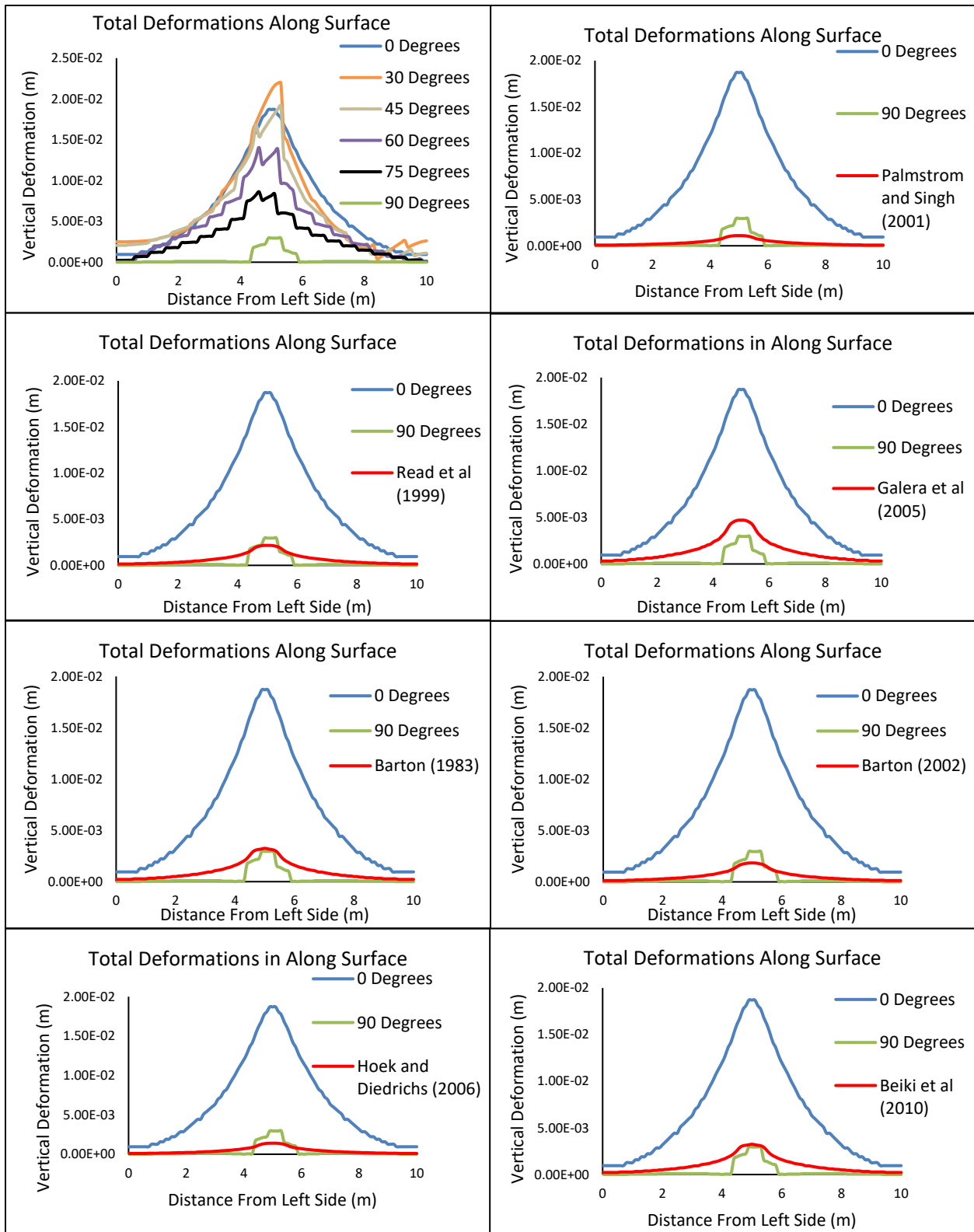


**Figure 4-5.** Maximum and minimum total deformations along the surface of each numerical model of RMR45 rock mass along with the predicted deformations by the selected empirical formulas Table (1-1).

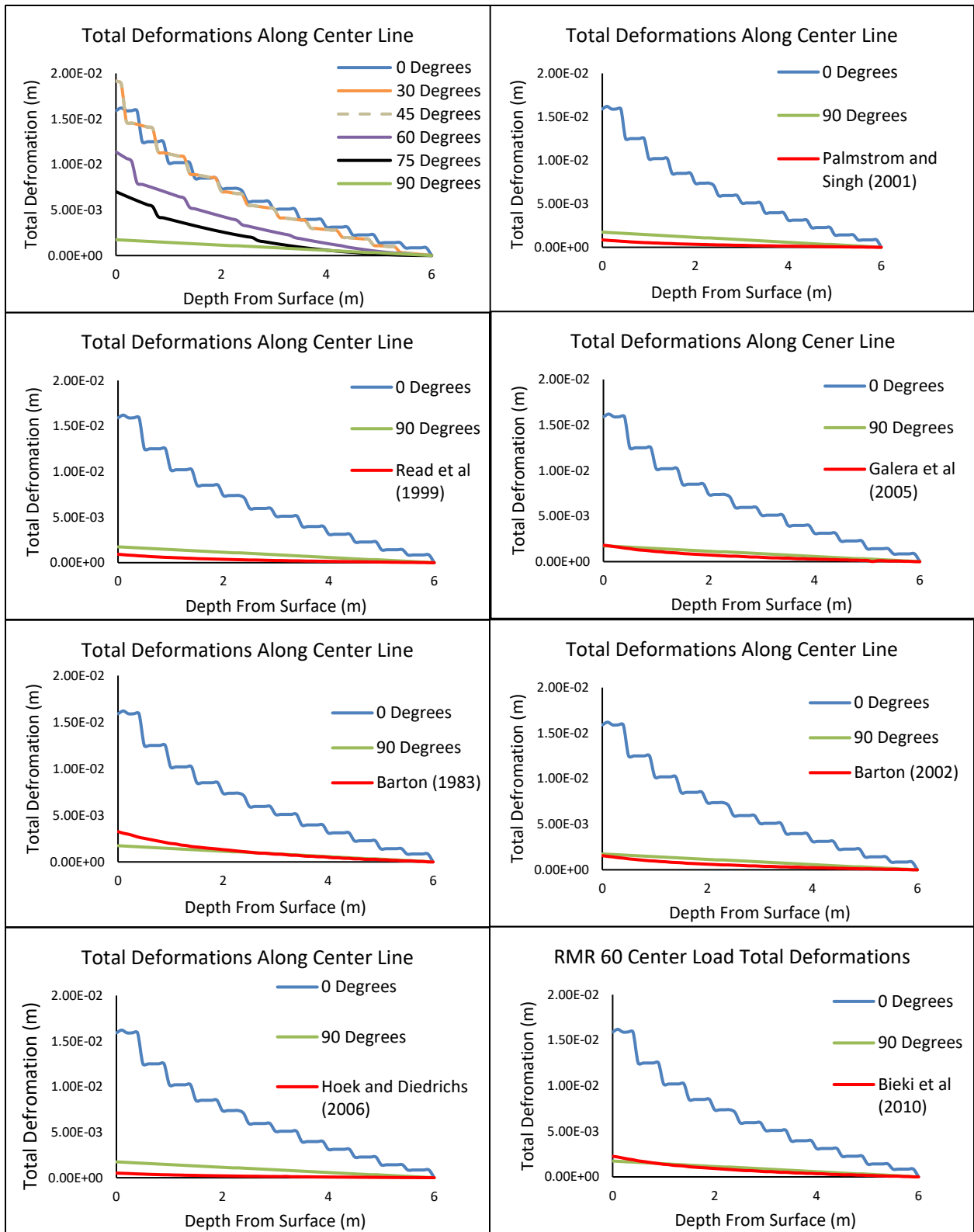


**Figure 4-6.** Maximum and minimum total deformations along the center line of the distributed load of each numerical model of RMR60 rock mass along with predicted deformations by the selected empirical formulas Table (1-1).

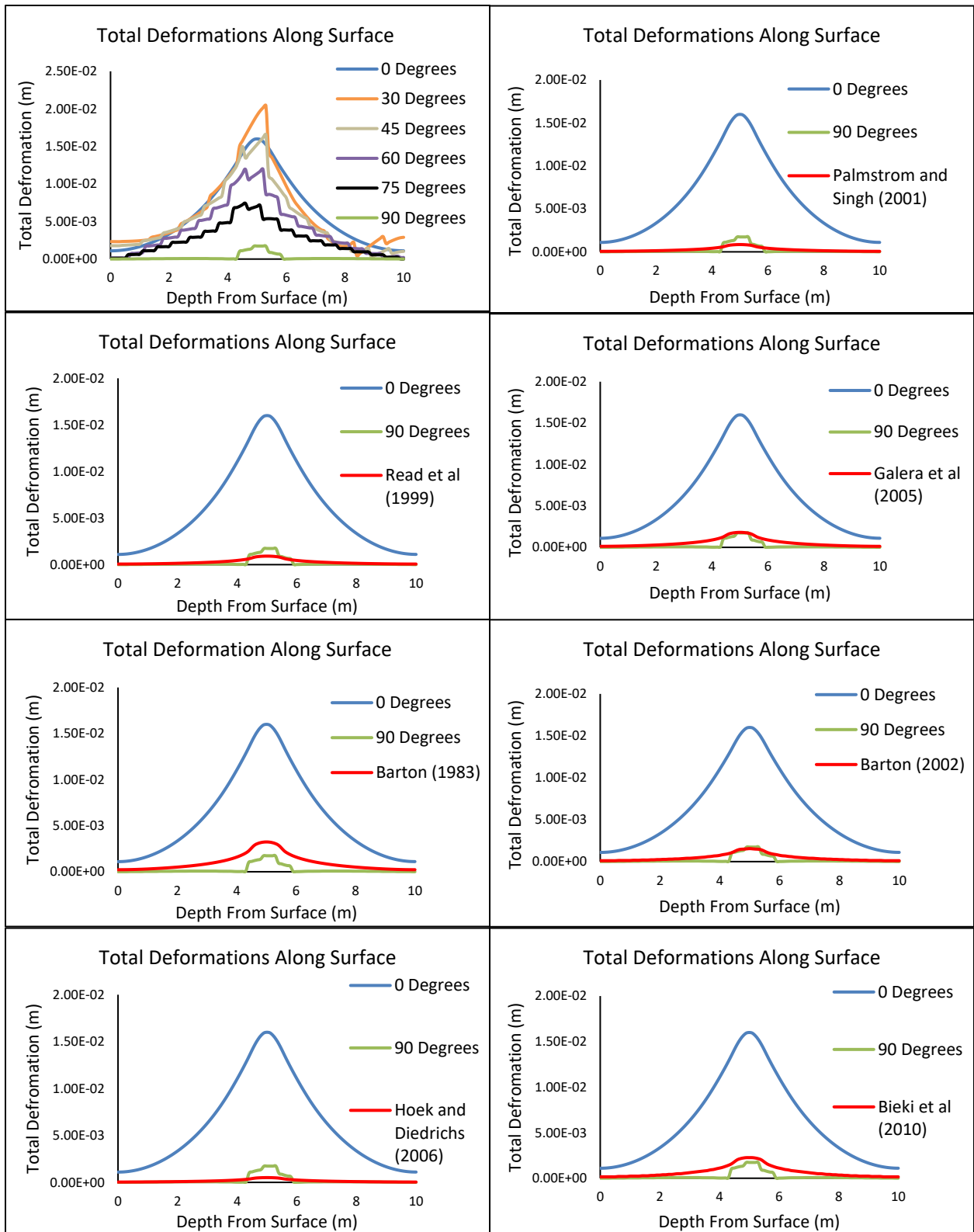


**Figure 4-7.** Maximum and minimum total deformations along the surface of each numerical model of RMR60 rock mass along with the predicted deformations by the selected empirical formulas Table (1-1).

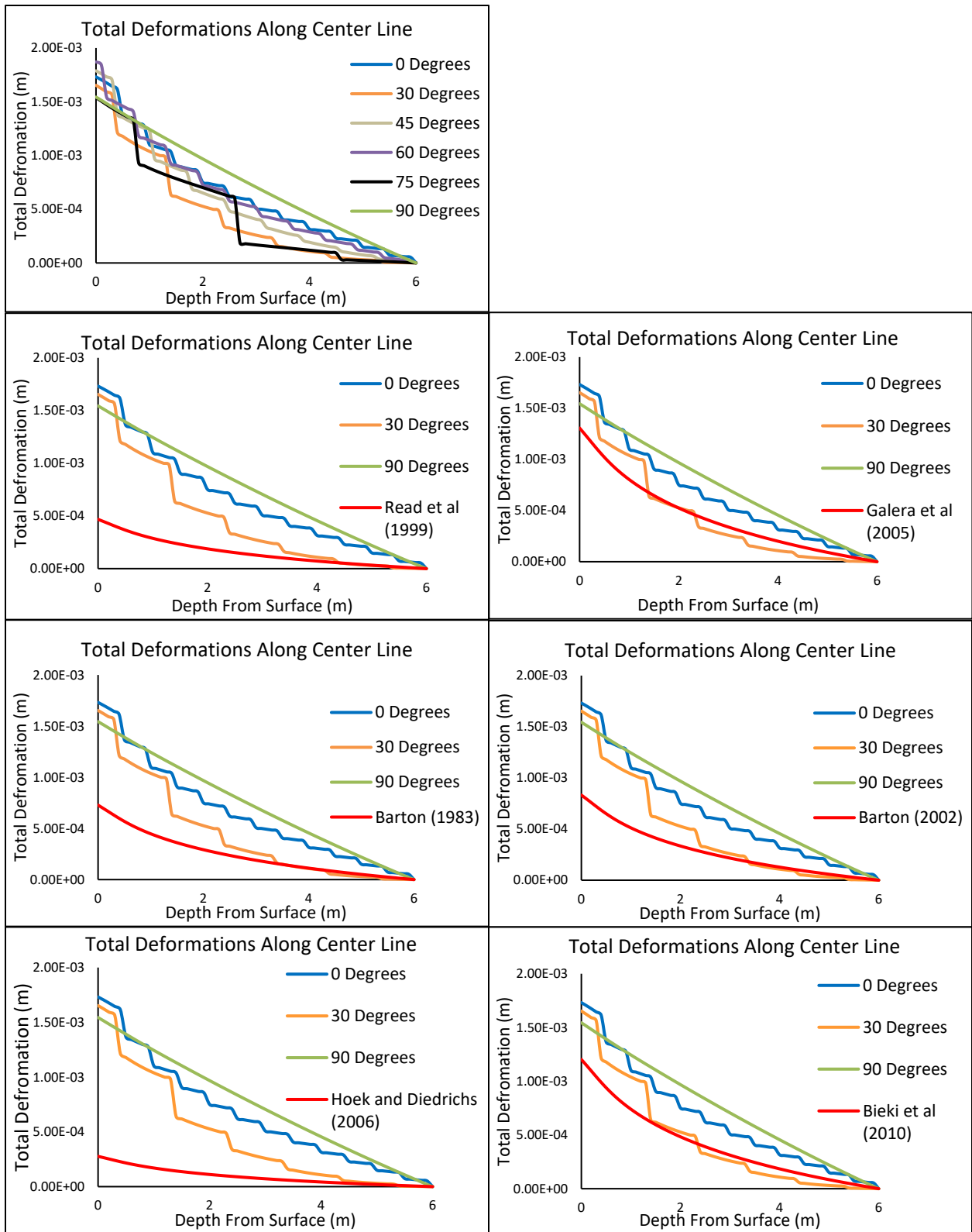


**Figure 4-8.** Maximum and minimum total deformations along the center line of the distributed load of each numerical model of RMR75 rock mass along with predicted deformations by the selected empirical formulas Table (1-1).

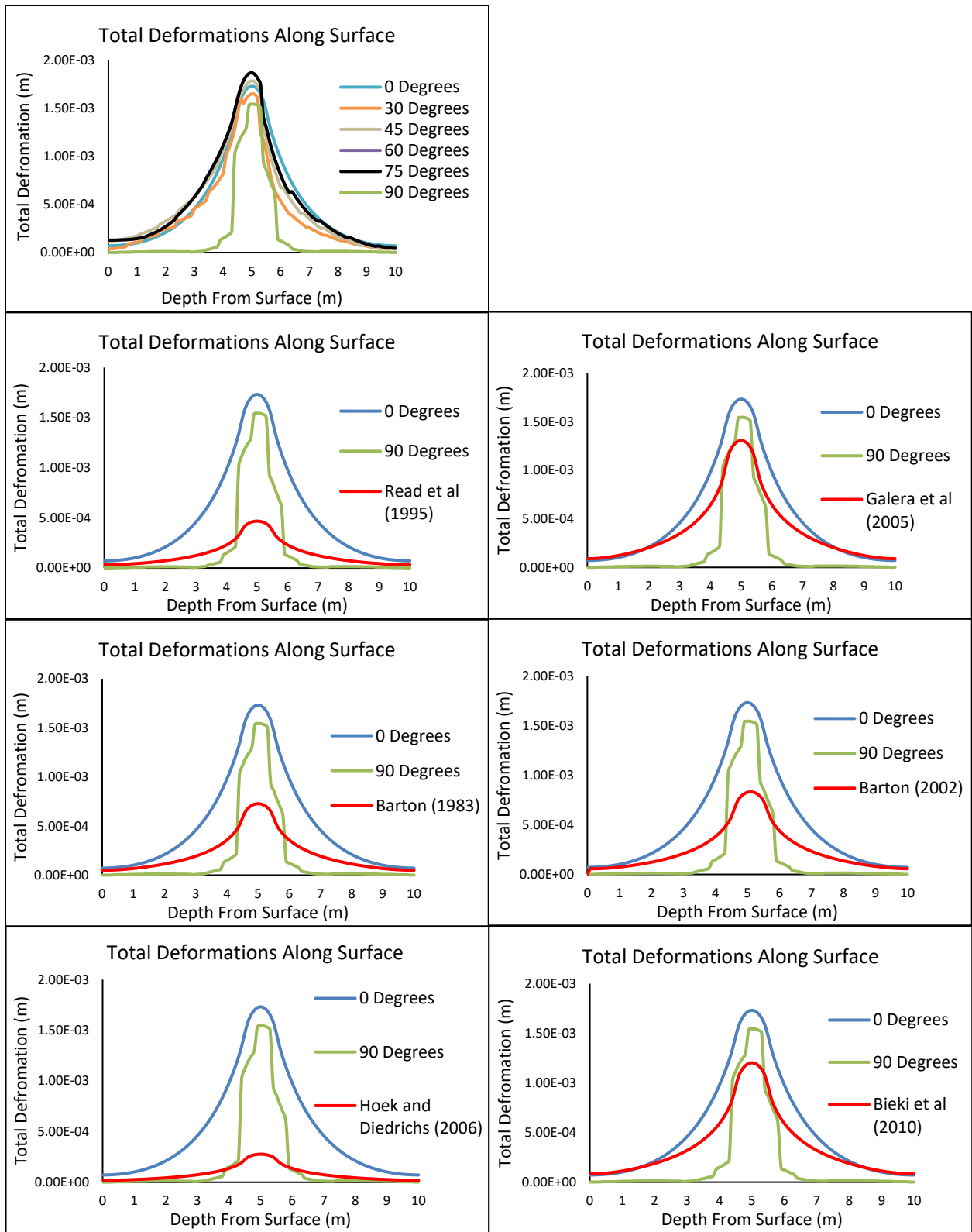


**Figure 4-9.** Maximum and minimum total deformations along the surface of each numerical model of RMR75 rock mass along with the predicted deformations by the selected empirical formulas Table (1-1).

## CHAPTER V CASE STUDY

### I. Geologic Setting

A road cut in Hardy Arkansas was modeled in RS2 as a case study (Fig. 5-1). The outcrop is located on highway 63 and is a part of the lower Ordovician aged Jefferson City – Cotter formation (Haley et al, 1993). The outcrop (Fig. 5-1) is approximately 10 m long and 4 m tall. A single fault and four other discontinuities are present in the rock mass.



**Figure 5-1.** Roadcut modeled in RS2.

The fault marks the boundary between a massive section of the rock mass (bottom) and a disintegrated section of the rock mass (top).

The Jefferson City – Cotter formation consist of two units, the Jefferson City and the Cotter, that are often indistinguishable from each other (Caplan, 1960). Both units contain oolitic cherts which help distinguish them from the Powell unit.

The Jefferson City dolomite is a fine grained to medium grained crystalline dolomite containing traces of cherts and dolomitic sandstone. Minor beds of sandstone or shale have also been found in this unit (Caplan, 1960). The Jefferson City Dolomite is estimated to range in thickness from 350 ft - 550 ft (Caplan, 1960).

The Cotter dolomite is generally indistinguishable from the Jefferson City dolomite due to the similarities in lithologies. In some boreholes a thin layer of sandstone or sandy dolomite marks the boundary between the two units. The Cotter unit is estimated to be 527 ft thick (Caplan, 1960).



**Figure 5-2.** Road cut with measured surfaces for discontinuity survey labeled.

## II. Building the In Situ Model

### *In situ measurements*

A discontinuity survey was conducted on the outcrop using a modified discontinuity survey sheet which can be found in Appendix B. This survey sheet contains all the required information to use all the RMCS discussed previously. For this survey the discontinuities found were a fault (FL), three separate joints (FR 1-3), and two bedding plane surfaces (BP 1-2) (Fig. 5-2). Results for the discontinuity survey can be found in the filled-out discontinuity sheet in appendix B. UCS was found for each surface using a L type Schmidt Hammer.

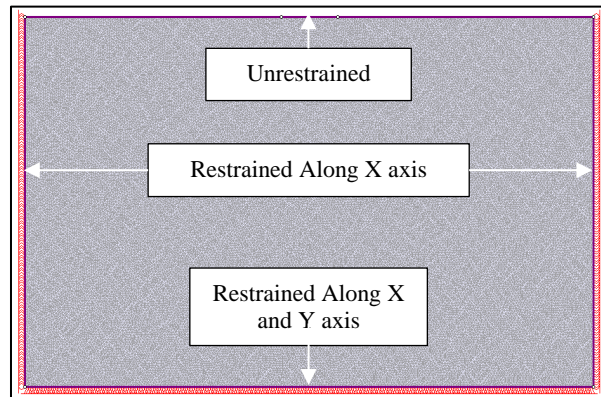


**Figure 5-3.** Stage 1 model with boundary conditions.

### *Stage 1 model Parameters*

Stage 1 of building the model consist of determining the size of the model, location and

magnitude of the applied load, and the properties of the fractured rock mass that exist above the fault.

A distributed load of 10 MPa was set in the middle of the upper boundary in order to simulate a bridge footing. The model size was set to be 10 m by 6 m in order to avoid the boundary effects on the formation of the pressure bulb. Boundary conditions were then set for each side of the model to simulate the conditions of an in situ rock mass (Fig. 5-3).

The Mohr-Coulomb strength criterion is used to define the strength of the fractured rock mass. A tilt table test of was used to determine the maximum

internal angle of friction. Cohesion values for the rock mass is derived from the GSI rating

found from the field survey. Since the material is modeled as plastic residual values need to be

found. For finding residual values the methods presented in Cai (2007) and the guidelines given by Crowder and Bawden (2004) are used. Cai (2007) gives as set of empirical formulas to determine residual GSI values from block volume, joint condition, joint weathering, joint surface rating, and joint alteration factor. Each of these variables are defined in the Rmi chart presented in Palmström (2001). Using this residual GSI calculated from Cai (2007) and the guidelines presented by Crowder and Bawden (2004) all of the residual values for the variables in the GSI system are found and presented in Table 5-1. From these residual GSI values it was possible to estimate the residual values for the Mohr – Coulomb criterion. The intact elastic modulus of the

Table 5-1. Peak and residual strength parameters for fractured rock

Parameters	Peak	Residual
$\sigma_c$	176.30	176.30
mb	0.25	0.19
s	$5.28 \times 10^{-5}$	$2.61 \times 10^{-5}$
a	0.52	0.52
mi	12.00	12.00
D	0.8	0.8
GSI	35	30
$\phi$	30.00	25.88
Cohesion (MPa)	4.03	3.33

Table 5-2. Ultrasonic pulse test results

Sample	$V_p$ (m/s)	$V_s$ (m/s)	$E_i$ (MPa)
1	5555.61	3330.25	71800
3	5648.65	3291.34	71760
4	5816.67	3877.78	88780
<b>Average</b>			<b>77450</b>

rock was found using ultrasonic pulse test on samples taken from the field site (Table 5-2).

### *Stage 2 Model Parameters*

Stage 2 of building the model consist of:  
adding the fault, modifying the boundary conditions, defining the properties of the relatively massive rock mass below the fault, and deciding the optimal mesh parameters as discussed in the last paragraph of this section (Fig. 5-4).

Using Image J software Figure 5-2 was scaled and the dimensions of the fault was found. The fault was mapped onto the model to locate the point where the fault will hit the top of the model. From there the dip found in the discontinuity survey was used to map the fault down to its lower most point. The ends of the joint element (which models the fault) are defined as “open” meaning that the end of the joint is represented by two nodes that can move with respect to each other.

When defining the joint properties, the slip criterion, joint normal stiffness, and joint shear stiffness need to be defined. The Barton- Bandis slip criterion was chosen due to the ease of determining the needed parameters (JCS, JRC, and

$\phi$ ) (Table 5-3). In determining JRC, criteria from the Q-system was used (Fig. 2-4): because the walls of the fault will not come in contact after 10 cm of shear due to the thickness of the filling (Fig. 5-5), it was decided to model the behavior of this fault by the properties of its filling

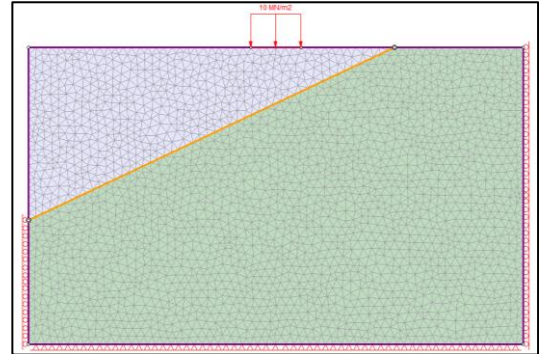


**Figure 5-4.** Stage 2 model. Fractured rock is shown in purple, massive rock in green, and the fault is shown by the orange line (Mesh size is reduced in order to display model features).



**Figure 5-5.** Kaolin infill of the fault.

material which is kaolinite. A Schmidt

hammer test was used to

Table 5-3. Parameters for discontinuities

Parameter	Discontinuity					
	FL	FR <sub>1</sub>	FR <sub>2</sub>	FR <sub>3</sub>	BP <sub>1</sub>	BP <sub>2</sub>
JCS (MPa)	34	162.5	162	52	87	87
JRC	6	15	5	13	7	7
Residual Friction Angle (Deg.)	25.88	25.88	25.88	25.88	25.88	25.88
K <sub>n</sub> (MPa/m)	51666	55963	55963	55963	55963	55963
K <sub>s</sub> (MPa/m)	20000	23514	23514	23514	23514	23514

fault. The lowest JRC value found was chosen since any failure along the fault would be facilitated by a failure along the smoothest portion. Normal and shear joint stiffness was found by using the formulas recommended by the RS2 publishers relating the normal and shear modulus (E and G respectively) of the infill material to the thickness of the material (H):

$$K_n = \frac{E}{H} \quad (5-1)$$

$$K_s = \frac{G}{H} \quad (5-2)$$

Normal and shear modulus values for unsaturated kaolin were taken from Parasad (2002) (Table 5-3).

Due to the presence of the fault the boundary condition of the model need to be modified; the leftmost boundary above the joint is changed to be unrestricted. This allows the top block to slide along the fault to the left.

Once again, the Mohr - Coulomb strength criterion is used for the lower portion of the model (Table 5-4). Since the massive rock mass is the same

Table 5-4. Peak and residual strength parameters for massive rock

Parameters	Peak	Residual
σ <sub>c</sub>	176.30	176.30
mb	1.49	0.19
s	4.98*10 <sup>-3</sup>	2.61*10 <sup>-5</sup>
a	0.52	0.52
mi	12.00	12.00
D	0.8	0.8
GSI	65	30
φ	30.00	25.88
Cohesion (MPa)	8.68	3.33

lithology as the fractured rock mass the same residual values were used.

A total of 23,245 elements are used in this model. The element type used for the mesh is a 6 noded triangle. A graded mesh is used allowing a greater concentration of nodes around the discontinuities within the model and the model's boundaries.

### *Stage 3 Model Parameters*

Stage three of building the model consist of adding in the three joints and two bedding planes described in the discontinuity survey. Mapping the discontinuities onto the model was done using the same methods discussed in stage 2.

For each of the discontinuities the Barton-Bandis criterion is used to define the remaining discontinuities for the same reasons described previously in stage 2 of the model. Since these discontinuities have less than 10 cm of filling the properties of these joints are more closely related to the properties of the intact rock. UCS was determined by using an L type Schmidt hammer on the walls of the joints. JRC and residual friction angle were found using the same methods outlined in the stage 2 section.  $K_n$  and  $K_s$  for these discontinuities are determined by using values provided for limestone by Barton (2006). Since all of the discontinuities exist in the same rock type these values are assumed to be the same for each discontinuity. Table 5-3 shows the values used to define each of these discontinuities.

### Testing the Models

In order to test each of the empirical predictions an isotropic FEM is created. For the isotropic model's intact properties, the properties of the fractured rock are used (Table 5-1). In this isotropic model the fractured rock mass properties are used in order to give a conservative estimate of deformations similar to what would be done in a real project setting. Then, the  $E_i$  of the fractured rock is replaced with the predictions of  $E_{rm}$  (Table 5-5). RMCS values are

determined using the same methods as

previously stated with RQD being derived using Image J software to determine the percentage of

rock pieces larger than 10 cm along

the portion of the road cut where the

center line of loading would be. Note

that this rock mass' R<sub>Mi</sub> value of 75 is

too high for the Palmström and Singh

(2001) formula to be used in this case

study.

Table 5-5 Predicted E<sub>rm</sub> for case study

Formulas	RMCS Value	Predicted E <sub>rm</sub> (GPa)
	<u>RMR</u>	
Read et al (1999)	63	25.0
Galera et al (2005)		28.0
	<u>Q</u>	
Barton (1983)	2.0	7.5
Barton (2002)		15.2
	<u>GSI</u>	
Hoek and Diederichs (2006)	58	22.0
Bieki et al (2010)		19.2

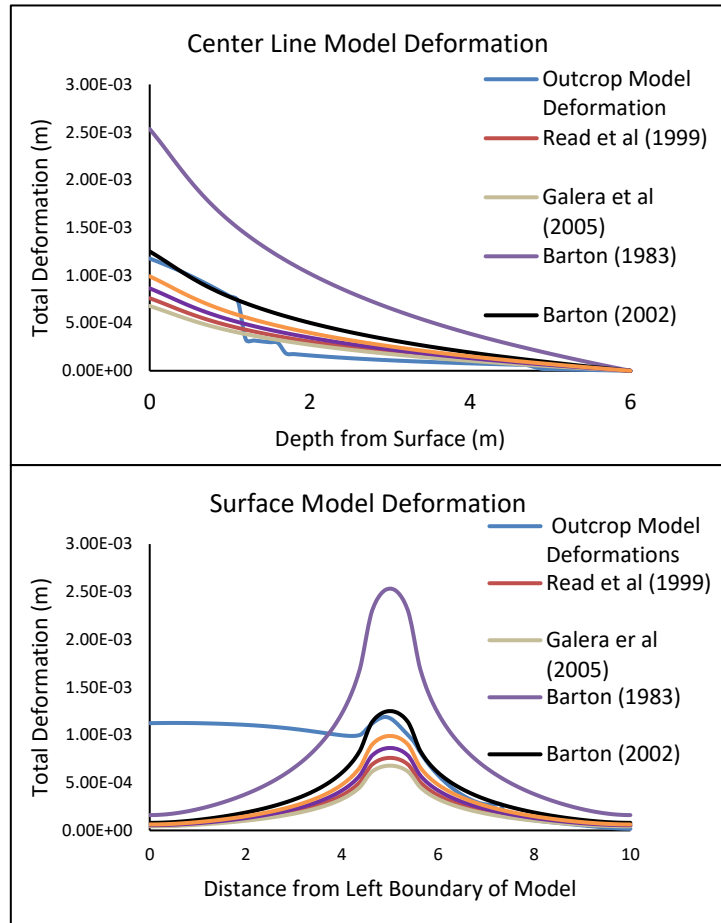
### III. Results and Discussion

Figure 5-6 shows resulting total deformations from each predicted model along with the deformations from the model of the outcrop. In this case study we can see that the deformations

of the modeled rock mass fall within the range of predicted deformations given by the six empirical formulas used. Barton (1983) predicts significantly higher deformations than the other formulas. Of the remaining formulas we can also see that the predicted results can be grouped by

RMCS. With formulas that use the Q system predicting the highest deformations, formulas using RMR predict the lowest deformations, and formulas using GSI having predictions that fall into the middle. Barton (2002) is nearly perfect when predicting the maximum deformations in this outcrop. Note that the actual outcrop model gives an asymmetric deformation profile whereas the formulas result in symmetric deformation profiles for equivalent homogeneous isotropic rock mass.

While Barton (2002) did prove to be the most accurate predictive method in this case study more case studies are needed to see if it was the Q system that led to a more accurate  $E_{rm}$



**Figure 5-6.** Total deformations for each predictive formula and the modeled outcrop.

prediction or if this result occurred by random chance. One result that does show the RMCS used has an effect on the final  $E_{rm}$  prediction is that each formula is grouped by their respective RMCS. This means that the RMCS used in a formula could have more effect on the final  $E_{rm}$  predicted than the structure of the formula itself..

CHAPTER VI  
DISCUSSION AND CONCLUSION

The stress bulbs predicted by Equations 3-12 to 3-14 (in Goodman, 1989) match the shape of the stress contours in the numerical models (Figure 4-4). Since these equations are validated by physical experiments on transversely isotropic models (Goodman, 1989), this match is confirmation that the methods outlined in this study lead to realistic numerical simulations of behavior of natural rock masses under surface loading. The reduction in loading for the RMR30 models to prevent their total yielding should not affect the validity of the conclusions derived from this study.

The lateral (surface) and vertical (center line) total displacement profiles presented in Figures 4-2 to 4-9 (Table 6-1) show that the maximum and minimum deformations appear to be random and not a simple function of

Table 6-1. Angles at which maximum and minimum deformations occurred in each model set.

Model Set	Angle for Maximum Deformation	Angle for Minimum Deformation
RMR30*	75°	60°
RMR45	30°	90°
RMR60	30° and 45°	90°
RMR75	60°	75°

\*RMR30 model with 90° could not converge.

the anisotropy angle. Therefore, it is reasonable to conclude that the deformations at any point within the zone of influence of surface load are a complex function of stiffnesses and frequency of the discontinuities as well as their orientation.

As the  $K_n/K_s$  ratio decreases and approaches 1, i.e., the value for isotropic rock masses, the difference between maximum and minimum deformations decreases at all angles of anisotropy as would be expected for isotropic media.

As rock mass quality changes so does the best performing predictive equation. However, there is no correlation between the rock mass quality and which predictive equation performs the best. While all formulas tend to predict lower than the minimum deformations in each set of numerical models there tends to be at least one formula that predicts within the range of numerically computed deformations for each set of models (with the exception of the RMR30 models where all predictive equations performed poorly). The best performing formula is different for each set of models (of a given rock mass quality) and does not relate to the formula's RMCS or to its mathematical structure. When looking at our case study we can see that the empirical predictions perform well in a rock mass with only one major discontinuity. The key difference between the case study and the synthetic models is the increased number of joints in the synthetic models.

Also, there are multiple instances where two formulas with different structures and different RMCS predict identical curves. If a single RMCS offered a more relevant set of parameters to predict  $E_{rm}$  then we would not expect to see this lack of consistency in a given RMCS performance. In all of our models not only do none of the formulas exhibit a clear advantage, most formulas consistently underpredict deformations (i.e., below the minimum) and no one formula consistently predicts deformations within the range that our numerical models deem possible.

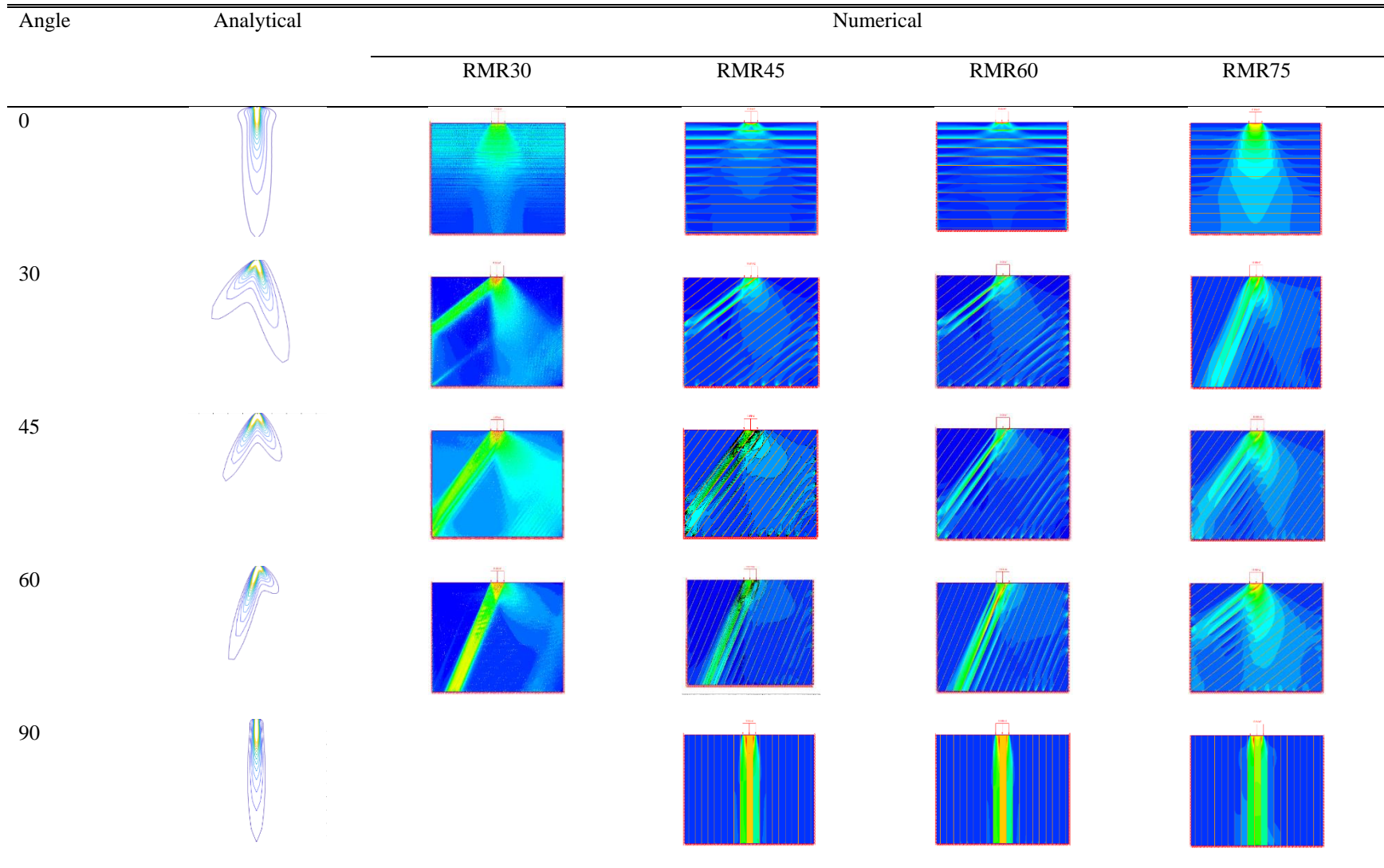
With these results it appears that the RMCS used in this study are insufficient as a base when used to derive empirical predictions for  $E_{rm}$ . This can be because of a lack of vital parameters or not giving certain parameters the appropriate weights when determining the final RMCS value. In this study we identified at least one underrepresented parameter and that is  $K_n$ . The effects of  $K_n$  can be seen in the changes in deformation as discontinuity angles change from

0° to 90° with all predictive formulas resulting in deformation values resembling rock masses with discontinuities oriented at 90°. In order to better predict  $E_{rm}$  of a rock mass, future research must more closely look at the effects of  $K_n$  and incorporate it either via a new RMCS or as an additional variable into the formulas.

This case study as well as the poor performance of the predictive formulas for the set of RMR\_30 models consistently reveals that although current RMCS do account for number of discontinuity sets and their spacing, the accuracy of the formulas decreases as the discontinuity frequency in the rock mass increases. This observation suggests that the frequency of discontinuities in a rock mass may be another parameter that should be better or more explicitly accounted in the predictive formulas.

# Appendix A

## Stress Patterns in Analytical and Numerical Solutions





## Bibliography

- Abad, J., Caleda, B., Chacon, E., Gutierrez, V., & Hidlgo, E. (1984). Application of geomechanical classification to predict the convergence of coal mine galleries and to design their supports. *5th International Congress Rock Mechanics*, (pp. 15-19). Melbourne.
- Agharazi, A., Tannant, D., & Martin, D. (2011). Characterizing rock mass deformation mechanisms during plate load test at the Bakhtiary dam project. *International Journal of Rock Mechanics and Mining Sciences*, *49*, 1-11. doi:10.1016/j.ijrmms.2011.10.002
- Amadei, B. (1996). Importance of Anisotropy When Estimating and Measuring In Situ Stresses in Rock. *International Journal of Rock Mechanics, Mining Sciences, and Geomechanics*, *9*, 293-325.
- Baguelin, F., Jézéquel, J., & Shield, D. (1978). *The pressuremeter and foundation engineering*. Clausthal: Trans Tech Publications.
- Bakhtar, K., & Barton, N. (1981). *Plate Load Testing at the Rocky Mountain Pumped Hydro Project*. Birmingham, AL: Southern Company Services Inc.
- Barton, N. (1984). Application of Q - system and index test to estimate shear strength and deformability of rock masses. *International Symposium of Engineering Geology and Underground Construction* (pp. 51-70). Lisbon: Laboratório Nacional de Engenharia Civ.
- Barton, N. (1995). The influence of joint properties in modelling jointed rock masses. *8th Congress of ISRM* (pp. 1023-1032). Tokyo: Balkema, Rotterdam.
- Barton, N. (2002). Some new Q - Value correlations to assist in site characterization and tunnel design. *International Journal of Rock Mechanics and Mining Sciences*, *39*, 185-216.
- Barton, N. (2006). *Rock Quality, Seismic Velocity, Attenuation and Anisotropy*. UK & Netherlands: Taylor & Francis.
- Barton, N., Lien, R., & Lunde, J. (1974). Engineering Classification of Rock Masses for the Design of Tunnel Support. *Rock Mechacnics*, *6*, 189-236.
- Beiki, M., Bashari, A., & Majdi, A. (2010). Genetic programming approach for estimating the deformation modulus of rock mass using sensitivity analysis by neural network. *International Journal of Rock Mechanics and*

- Mining Sciences*, 47, 1091-1103. doi:10.1016/j.ijrmms.2010.07.007
- Bieniawski, Z. (1978). Determining Rock Mass Deformability: Experience from Case Histories. *International Journal of Rock Mechanics, Mining Sciences, and Geomechanics Abstracts*, 237-247.
- Bieniawski, Z. (1989). *Engineering Rock Mass Classification A Complete Manual for Engineers and Geologists in Mining, Civil, and Petroleum Engineering*. New York: Wiley-Interscience.
- Bieniawski, Z. (1989). *Engineering Rock Mass Classifications*. New York: Wiley.
- Boyle, W. (1992). Interpretation of Plate Load Test Data. *International Journal of Rock Mechanics, Mining Sciences, and Geomechanics Abstracts*, 29, 133-141.
- Cai, M., Kaiser, P., Tasaka, Y., & Minami, M. (2007). Determination of residual strength parameters of jointed rock masses using the GSI system. *International Journal of Rock Mechanics and Mining Sciences*, 44, 247-265. doi:10.1016/j.ijrmms.2006.07.005
- Cameron-Clarke, I., & Budavri, S. (1981). Correlation of rock mass classification parameters obtained from borecore and in-situ observations. *Engineering Geology*, 17, 19-53.
- Caplan, W. (1960). *Subsurface Geology of Pre - Everton Rocks in Northern Arkansas*. Little Rock: Arkansas Geological Survey.
- Cia, M. (2006). Visualization of rock mass classification systems. *Geotechnical and Geological Engineering*, 41, 1089-1102.
- Cia, M., Kaiser, P., Uno, J., Tasaka, Y., & Minami, M. (2004). Estimation of rock mass strength and deformation modulus of jointed hard rock masses using the GSI system. *Rock Mechanics and Mining Sciences*, 41, 3-19.
- Crowder, J., & Bawden, W. (2004). *Review of Post-Peak Parameters and Behavior of Rock Masses: Current Trends and Research*. Retrieved from rocscience: [https://www.rocscience.com/documents/pdfs/rocnews/fall2004/Crowder\\_Bawden.pdf](https://www.rocscience.com/documents/pdfs/rocnews/fall2004/Crowder_Bawden.pdf)
- Deer, D., Hendron, A., Patton, F., & Cording, E. (1967). Design of surface and near surface construction in rock. *8th U.S. Symposium Rock Mechanics* (pp. 237-302). New York: Society of Mining Engineers.

- Gage, J., Dante, F., Turner, A., MacLaughlin, M., & Wang, H. (2013). Validation and implementation of a new method for monitoring in situ strain and temperature in rock masses using fiber-optically instrumented rock strain and temperature strips. *International Journal of Rock Mechanics*, 61, 244-255.  
doi:10.1016/j.ijrmms.2013.03.007
- Gage, J., Wang, H., Fratta, D., & Turner, A. (2014). In situ measurements of rock mass deformability using Bragg grating strain gauges. *International Journal of Rock Mechanics and Mining Sciences*, 71, 350-361.  
doi:10.1016/j.ijrmms.2014.07.021
- Galera, J., Álvarez, M., & Bieniawski, Z. (2005). Evaluation of the deformation modulus of rock masses using RMR. Comparison with dilatometer test. *Proceedings of ISP5-PRESSIO*. Paris.
- Goodman, R. (1989). *Introduction to Rock Mechanics Second Edition*. New York: John Wiley & Sons Ltd.
- Goodman, R., Taylor, R., & Brekke, T. (1968). A model for mechanics of jointed rock. *Journal of the Soil Mechanics and Foundations Division*, 94, 637-659.
- Grimstad, E., & Barton, N. (1993). Updating the Q System for NMT. *International Symposium of Sprayed Concrete-Modern Use of Wet Mix Sprayed Concrete for Underground Support* (pp. II.51-II.70). Fagernes, Oslo: Norwegian Concrete Association.
- Hack, R., & Price, D. (1997). Quantification of weathering. *Engineering Geology and the Environment*, 145-150.
- Haley, B., Ernest, G., Bush, W., Clardy, B., Stone, C., Woodward, M., & Zachary, D. (1993). *Geologic Map of Arkansas*. Little Rock: Arkansas Geological Survey.
- Hammah, R., Yacoub, T., Corkum, B., & Curran, J. (2008). The Practical Modelling of Discontinuous Rock Masses with Finite Element Analysis. *42nd US Rock Mechanics Symposium*. San Francisco: American Rock Mechanics Association.
- Hoek, E., & Diederichs, M. (2005). Empirical estimation of rock mass modulus. *International Journal of Rock Mechanics and Mining Sciences*, 43, 203-215. doi:10.1016/j.ijrmms.2005.06.005
- Hoek, E., & Marinos, P. (2000). Predicting tunnel squeezing problems in weak heterogeneous rock masses. *Tunnels and Tunnelling International*, 1-21.

- Hoek, E., Carter, T., & Diederichs, M. (2013). Quantification of the Geological Strength Index Chart. *47th US Rock Mechanics/Geomechanics Symposium* (pp. 1-9). San Francisco, CA: NGI Publication.
- Hoek, E., Kaiser, P., & Bawden, W. (2000). *Support of Underground Excavations in Hard Rock*. CRC Press.
- Hok, K. (2001). Review of Menard Pressuremeter Test in Weak Rock [Masters Thesis]. *Univeristy of Hong Kong*, 40.
- ISRM. (International Journal of Rock Mechanics, Mining Sciences, and Geomechanics Abstracts). 1979. *Suggested Method for determination of in situ deformability of rock*, 16, 6-143.
- Ivars, D., Pierce, M., Darcel, C., Reyes-Montes, J., Potyondy, D., Yound, R., & Cundall, P. (2011). The synthetic rock mass approach for jointed rock mass modelling. *International Journal of Rock Mechanics and Mining Sciences*, 48, 219-244. doi:10.1016/j.ijrmms.2010.11.014
- Jianping, Y., WeiZhong, C., DianShen, Y., & JingQiang, Y. (2015). Numerical determination of strength and deformability of fractured rock mass by FEM modeling. *Computers and Geotechnics*, 64, 20-31. doi:10.1016/j.compgeo.2014.10.011
- Kayabasi, A., & Gokceoglu, C. (2018). Deformation Modulus of Rock Masses: An Assesment of the Existing Empirical Equations. *Geotechnical and Geological Engineering*, 36, 2683-2699. doi:10.1007/s10706-018-0491-1
- Kulatilake, P., Shreedharam, S., Sherizadeh, T., Shu, B., Xing, Y., & He, P. (2016). Laboratory Estimaiton of Rock Joint Stiffness and Frictional Parameters. *Geotechnical and Geological Engineering*, 34, 1723-1735. doi:10.1007/s10706-016-9984-y
- Kumar, N., Samadhiya, N., & Anbalagan, R. (2004). Application of rock mass classification system for tunneling gin Himalaya. *International Journal of Rock Mechanics and Mining Sciences*, 41, 852-857. doi:10.1016/j.ijrmms.2004.03.147
- Li, D., Wong, L., Liu, G., & Zhang, X. (2012). Influence of water content and anisotropy on the strength and deformability of low porosity meta-sedimentary rocks under triaxial compression. *Engineering Geology*, 46-66.

- Lo, K., & Hefny, A. (2001). Foundations on Rock. In *Geotechnical and Geoenvironmental Engineering Handbook* (pp. 305-332). Boston, MA: Springer. doi:10.1007/978-1-4615-1729-0\_11
- Lo, K., & Lukajic, B. (1984). Predicted and Measured Stresses and Displacements Around the Darlington Intake Tunnel. *Canadian Geotechnical Journal*, 21, 147-165.
- Moreno, R. (2019, July). *What does shape function mean in finite element formulation?: What does shape function mean in finite element formulation?* Retrieved from Stochasticandlagrangian.blogspot.com:  
<http://stochasticandlagrangian.blogspot.com/2011/07/what-does-shape-function-mean-in-finite.html>
- Palmström, A. (1995). RMI - A for rock mass characterization system for engineering purposes [Ph.D. thesis]. *University of Oslo, Norway*, 400.
- Palmström, A. (1996). RMI - a system for characterizing rock mass strength for use in rock engineering. *Journal of Rock Mechanics and Tunneling Technology*, 1, 69-108.
- Palmström, A., & Singh, R. (2001). The deformation modulus of rock masses - comparisons between in situ test and indirect estimates. *Tunnelling and Underground Space Technology*, 16, 115-131.
- Prasad, M., Kopycinska, M., Rabe, U., & Arnold, W. (2002). Measurement of Young's modulus of clay minerals using atomic force acoustic microscopy. *Geophysical Research Letters*, 29, 1-4.  
doi:10.1029/2001GL014054
- Read, S., Richards, L., & Perrin, N. (1999). Applicability of the Hoek-Brown failure criterion to New Zealand greywacke rocks. *Proceedings fo the nineth international congress on rock mechanics*, 2, pp. 655-660. Paris.
- Rezaei, M., Ghafoori, M., & Ajalloeian, R. (2016). Comparison between the In Situ Test's Data and Empirical Equations for Estimation of Deformation Modulus of Rock Mass. *Geosciences Research*, 1, 47-59.  
doi:10.22606/gr.2016.11005
- Russo, G. (2007). Improving reliability of GSI estimation: the intergrated GSI - RMI system. *ISRM Workshop Underground Works under Special Conditions*, (pp. 103-111). Madrid.
- Russo, G. (2009). A new rational method for calculating the GSI. *Tunneling and Underground Space Technology*,

24, 103-111.

Rutledge, J., & Preston, R. (1978). Experience with engineering classifications of rock. *Proceedings of International Tunneling Symposium*, (pp. A3.1-A3.7). Tokyo.

Saroglou, C., Qi, S., Guo, S., & Wu, F. (2018). ARMR, a new classification system for the rating of anisotropic rock masses. *Bulletin of Engineering Geology and the Environment*, 1-16.

Saroglou, H., & Tsiambaos, G. (2008). A modified Hoek - Brown failure criterion for anisotropic intact rock. *International Journal of Rock Mechanics and Mining Sciences*, 45, 223-224.

Saxena, K., & Sharma, V. (2002). *In-situ Characterization of Rocks*. CRC Press.

Shen, J., Karakus, M., & Xi, C. (2012). A comparative study for empirical equations in estimating deformation modulus of rock masses. *Tunneling and Underground Space Technology*, 32, 245-250.  
doi:10.1016/j.tust.2012.07.004

Sonmez, H., & Ulusay, R. (1999). Modifications to the geological strength index (GSI) and their applicability to the stability of slopes. *International Journal of Rock Mechanics and Mining Sciences*, 36, 743-760.

Voegele, M., Hardin, E., Lingle, D., Board, M., & Barton, N. (1981). *Site Characterization of Joint Permeability Using the Heated Block Test*. Salt Lake City: Terra Tek, Inc.

Zhang, L. (2016). Evaluation of rock mass deformability using empirical methods - A review. *Underground Space*, 2, 1-15.

VITA

**Tanner C. Avery**

---

**Education**

---

University of Mississippi Oxford, Mississippi

Masters of Science in Geological Engineering August 2018 – May 2020

- Thesis: The effects of rock mass classification schemes on predicting rock mass deformation modulus
- 3.65/4.00 Graduate GPA

Georgia Southern University Statesboro, Georgia

Bachelor of Science in Geology August 2014 - May 2018

- Senior Thesis: Seasonal Changes in Submarine Groundwater Discharge in a Salt Marsh Estuary: Saint Simons Island, Georgia.
- 3.76/ 4.00 cumulative GPA
- Graduated Magnum Cum Laude
- Graduated from University Honors Program

---

**Work Experience**

---

Geophysics Teaching Assistant Oxford, Mississippi

University of Mississippi January 2018 – May 2020

Hydrogeology Teaching Assistant Oxford, Mississippi  
University of Mississippi August 2018 – December 2019

Geology Tutor Statesboro, Georgia  
Georgia Southern University August 2017 – May 2018

Research Assistant Saint Catherines Island, Georgia  
Georgia Southern University March 2017 – May 2018

---

### Grants and Awards

---

Outstanding Graduate Student Award March 2020

- An award voted on by the faculty of geology and geological engineering department at the University of Mississippi given to a single graduate student within the department

Charles King Memorial Scholarship January 2020

- A \$1,500 scholarship awarded to a graduate student in the department of geology and geological engineering in memory of Charlie King.

Summer Research Assistantship June 2019 – August 2019

- Awarded a \$2,500 scholarship by the University of Mississippi to continue my thesis research through the summer

Teaching Assistantship August 2018 – Present

- A \$7,000 per semester stipend to teach one upper level undergraduate lab a semester while attending classes

University Honors Student May 2016 – May 2018

- Accepted as a member of and graduated from Georgia's Southern's Honors Program

Field Camp Scholarship April 2018

- \$1,000 scholarship for University of Missouri Field Camp from the Garvin and Johnson Memorial fund

Zell Miller Scholarship August 2014 – May 2018

- Full tuition scholarship awarded to Georgia high school students who graduate with a GPA of 3.7 with an ACT of at least 26 and maintain a minimum of a 3.2 GPA in college.

College of Undergraduate Research Grant May 2017

- \$1,500 grant for senior thesis research from Georgia Southern University.

Henderson Scholarship

May 2017

- \$1,500 scholarship awarded to one geology major from Georgia Southern every year.

President's List

Spring 2015, Fall 2015, Spring 2017, Fall 2017

- Awarded to students enrolled 12 or more credit hours and make a term GPA of 4.0 at Georgia Southern University

Dean's List

2016

- Awarded to students enrolled 12 or more credit hours and make a term GPA of 3.5-3.9 at Georgia Southern University

Brett Warren Memorial Scholarship

May 2014

- \$500 scholarship given to the most academically successful athlete to graduate each year from Dade County High School